An International Journal of Optimization and Control: Theories & Applications
ISSN: 2146-0957 eISSN: 2146-5703
Vol. 16, No. 3, pp.1023-1048 (2026)
https://doi.org/10.36922/IJOCTA026040014

RESEARCH ARTICLE

Effective suppression of broadband disturbances using a dual-loop stabilization system

Vadim Zhmud[1,2*] and Lubomir Dimitrov[3,4]

[1] Department of Electronic Laser Systems, Institute of Laser Physics of the Siberian Branch of the Russian Academy of Sciences, Novosibirsk, Russia
[2] Department of Monitoring of Crustal Deformations, Altai-Sayan branch of the Federal State Budgetary Institution of Science Geophysical Service of the Russian Academy of Sciences, Novosibirsk, Russia
[3] Faculty of Mechanical Engineering, Technical University of Sofia, Sofia, Bulgaria
[4] Laboratory Mechatronic Systems for Discrete Manufacturing Processes, Centre of Competence MIRACle, Sofia, Bulgaria
vadim@laser.nsc.ru; Lubomir_dimitrov@tu-sofia.bg

ARTICLE INFO

Article history:
Received: January 24, 2026
Revised: March 6, 2026
Accepted: March 12, 2026
Published Online: May 6, 2026

Keywords:
Proportional–integral–derivative
Frequency stabilization
Motion separation
Numerical optimization
Mathematical modeling

AMS Classification 2010:
90B23, 90B56

ABSTRACT

This article proposes a solution to the problem of suppressing broadband disturbances acting on a controlled object. These disturbances include large low-frequency components and small to medium-frequency components. The paper presents the development of an existing approach that uses two methods to influence the output variable. It is proven that a fundamental property of different control loops is the mandatory intersection of their logarithmic amplitude–frequency characteristics at the frequency corresponding to the boundary between the influence ranges of these loops. This is achieved only if these characteristics have different slopes in this region. Consequently, the slow loop must take the form of a higher-order filter than the fast loop. On this basis, it is demonstrated that the order of the slow loop should be second or higher, while the order of the fast loop is preferably first order. The effectiveness of the method is demonstrated, for the first time, through simulation, including cases with third- and fifth-order transfer functions for the slow loop.

1. Introduction

Negative feedback systems are widely used in various technical devices. Feedback stabilizes the frequency of the laser radiation, reducing the deviation of the laser-generated frequency from the characteristic minimum of light absorption by the reference absorbing medium to zero.

In a study by Wu *et al.*,[1] an automatic frequency stabilization system with an external resonator cavity was developed for a 780 nm semiconductor laser using a commercial data-acquisition board. This system is based on the saturated absorption spectrum of rubidium atoms and is coupled to a commercial data acquisition board.

In another study, a method for laser frequency stabilization based on the linear dichroism signal in a transverse magnetic field was proposed; the method was used to stabilize the laser frequency near a low-frequency transition in the cesium D1 line.[2]

Jin *et al.*[3] reported a portable self-excited atomic magnetometer based on cesium pumped by a vertical-cavity surface-emitting laser; the work aims to miniaturize the stabilized laser.

* Corresponding Author

Singh *et al.*[4] proposed a laser frequency stabilization scheme and demonstrated magnetically induced dichroism measurements in an atomic vapor for a weak probe laser beam in the presence of a counter-propagating strong pump laser beam. Rubidium was also used as a reference. Zhao *et al.*[5] reported the frequency of a semiconductor laser was locked to the D1 transition line of rubidium atoms using a frequency-stabilization system based on modulation transfer spectroscopy.

Jeong *et al.*[6] experimentally and theoretically investigated the optimal conditions for polarization spectroscopy for laser frequency stabilization at various pump beam intensities and temperatures in rubidium vapor.

Beica *et al.*[7] provide a review of experiments on laser spectroscopy and atom trapping, discussing the experimental details and their impact on stabilization accuracy.

Kim *et al.*[8] describe the simultaneous frequency stabilization of two diode lasers with an external cavity at 780 nm using a precision wavelength meter.

Wang *et al.*[9] describe a technology for frequency stabilization of a multi-wavelength, narrow-beam laser based on a Fabry–Perot etalon. This technology utilizes digital frequency control, providing stable reference frequencies for various lasers. This increases the system's flexibility and adaptability.

A scientific review by Liu *et al.*[10] presents several methods for stabilizing laser frequency at significant distances from resonance and discusses existing challenges and possible directions for further research in this area.

Bengalskii *et al.*[11] propose a new method for measuring laser phase noise and frequency stability based on phase-sensitive optical time-domain reflectometry. In this method, the laser under study is used in a phase-sensitive optical time-domain reflectometer that employs phase-modulated double pulses and acts as an optical frequency discriminator.

In a study by Wu *et al.*,[12] to achieve high-frequency stability of an external cavity diode laser, a 780 nm diode laser is used as the pump source, with its frequency precisely synchronized with the saturated absorption peak of rubidium atoms using modulation transfer spectroscopy.

Fan *et al.*[13] proposed an approach to rapid frequency stabilization based on an improved mean-shift algorithm and tested it on a proprietary laser system to accelerate the frequency stabilization process in the event of unexpected interruptions.

The problem of precise dual-frequency control of lasers in airborne coherent Doppler lidar systems is addressed by implementing an innovative laser driver architecture that combines a compact hardware design with cascaded proportional–integral–derivative (PID) control and a frequency-temperature compensation mechanism.[14]

Wei *et al.*[15] showed that a 319 nm ultraviolet laser with a narrow linewidth, high frequency stability, and high output power is required for single-stage Rydberg excitation of cesium atoms. This study utilizes nonlinear frequency conversion technology.

Bagaev *et al.*[16] reported that a 3.39 μm helium-neon laser is frequency-locked to the methane clearing line, resulting in a spectral width of 7 Hz. Additionally, a stabilized laser is used to study the frequency properties of muonium produced at a particle accelerator.[17]

Furthermore, a multichannel phase-compensated active control for disturbance suppression is proposed, incorporating an improved feedback strategy for handling phase lag in an extended state observer and residual uncertainty in the system.[18]

New approaches to laser frequency stabilization are proposed and justified.[19]

For example, a Helium–Neon (He–Ne) laser with a wavelength $\lambda \approx 3.39\ nm$ can be locked to the methane absorption line near this frequency, which exhibits stability of more than fifteen orders of magnitude.[16,17] The task of such a stabilization system is to suppress uncontrolled deviations in the laser radiation frequency from the prescribed state, caused by various factors. These deviations are referred to as disturbances. The spectrum of such disturbances is quite broad, including slow-frequency drifts due to thermal and other slow processes, medium-frequency drifts caused by the power supply, ground and building vibrations, operation of neighboring installations, and disturbances at sound frequencies propagating through structures and air.[16,17] Even with all possible technical means to reduce these phenomena, residual disturbances can cause laser frequency deviations, which, in the absence of feedback, may reach up to 1 MHz for slow deviations.

A simplified diagram of the system is shown in **Figure 1**. The active medium, through which current passes, generates light radiation and amplifies the radiation entering it, enabling the latest generation of lasers. Mirror 1 and semitransparent mirror 2 form the laser resonator. The distance between the mirrors affects the radiation frequency. Piezoelectric modulators 1 and 2 enable the mirrors to be moved and the radiation frequency to

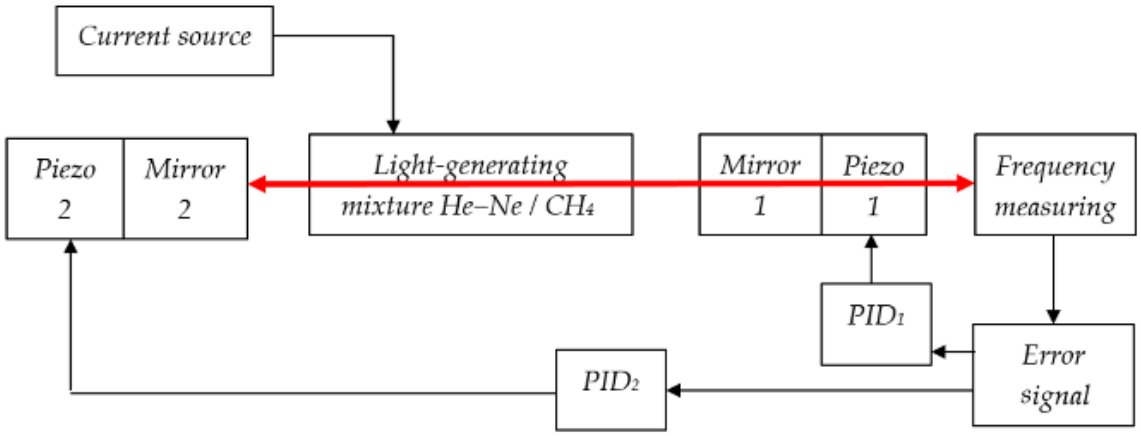

Figure 1. Simplified diagram of the laser frequency stabilization system. Abbreviations: CH_4: Methane; He: Helium; Ne: Neon; PID_2: Second proportional–integral–derivative.

be varied within the active medium's gain circuit. They are used to stabilize the frequency.[16,17]

These plate-shaped devices, based on the piezoelectric effect, change their thickness in response to an electric current, allowing one of the laser mirrors to be moved and lengthening or shortening its optical length by several micrometers. However, the problem is that the large deflections required to suppress large disturbances can be achieved only with a stack of several piezoelectric plates bonded together. These plates have a relatively large diameter compared to the light beam, which, in this case, cannot provide the required high deflection speed. A slow modulator can be designed with a hole in the center to allow the beam to pass through to the laser output. Using only a single small-diameter piezoelectric plate with a small mirror significantly increases the speed of this device, but the achievable range of mirror displacements remains insufficient.

When solving this problem, it is useful to consider that large perturbations have only relatively low velocities, while high-frequency perturbations have relatively small amplitudes. This led to the idea of using two different piezoelectric modulators, especially since the laser uses two mirrors. One modulator should suppress slow, large deviations in laser frequency, while the other should suppress fast, small deviations.[16,17]

To implement this idea, it is not enough to simply configure two modulators with the required amplitude and frequency differences to affect the laser frequency. It is also necessary to ensure that the modulators perform their intended task accurately.

Early implementations of this idea failed to provide a proper solution to this technical and mathematical problem. In their designs, the amplitude–frequency characteristics of the two paths, slow and fast, were proportional to each other in the frequency range where they were supposed to provide disturbance suppression.[16,17] On a logarithmic scale, this means the two transfer characteristics were parallel.

Theoretical analysis, supported by calculations, showed that these graphs must intersect because the amplitude–frequency characteristic of each loop must be significantly greater than that of the other within the frequency range in which that loop is intended to suppress the corresponding component of the laser-frequency disturbance spectrum.[16,17] In this case, the theory predicts that these transfer functions must have different orders (that means different slopes).

For the system to be stable, the high-frequency portion of its overall transfer function must intersect the frequency axis at an angle no steeper than −20 dB/dec, which corresponds to a first-order transfer function. This slope must be ensured by the transfer function of the fast stabilization loop. For this reason, the transfer function of the fast channel must have the properties of a first-order transfer function in this frequency range, while the transfer function of the slow channel must have the properties of a second-order or higher transfer function in the frequency range where these two functions intersect.

Accordingly, the slope of this characteristic on a logarithmic scale must be −40 dB/dec or steeper, for example, −60 dB/dec, −80 dB/dec, and so on, which corresponds to second-order, third-order, fourth-order, and so on.

The peculiarity of this situation is that such a system cannot operate solely with a slow channel, as that would lead to instability. If the system were stable solely with a slow channel, the intended idea would fail, as the aforementioned curves would then be parallel and, consequently,

either comparable in magnitude over a wide frequency range, or one of these curves would be significantly higher than the other across this entire frequency range. In the first case, both circuits would contribute equally to disturbance suppression across this entire frequency range. In the second case, suppression would be achieved by the loop with the significantly greater characteristic, while the second loop would contribute almost nothing to disturbance suppression, and it would therefore be ineffective, simply a redundant device.

These results are based on effective experimental and theoretical research into modifying stabilization systems to improve their accuracy, with a critical analysis of the technical solutions of predecessors who developed this idea but, unfortunately, did not establish the patterns described above, which resulted in parallelism in the characteristics of these two loops and the ineffectiveness of this idea in practice.

The reason for this error is that the system's creators developed and configured the systems separately—the slow loop separately, the fast loop separately—and then activated both. They reasoned that if the slow loop is stable and suppresses the slowest disturbances, as confirmed by testing, and the fast loop effectively suppresses small, fast disturbances, as also confirmed by testing, then using them together would achieve the desired result. In practice, no one has verified that both factors are sufficiently effective.

Our testing revealed this problem. The problem is that the control signal supplied to the slow piezoelectric modulator contains signals of all frequencies, both slow and fast, while the control signal supplied to the fast piezoelectric modulator has a low amplitude across the entire frequency range. Naturally, the amplitude comparison was performed using the coefficients for the voltage effect on the displacement of the corresponding mirror. If the gain of the slow circuit is increased, then it will contain not only relatively high-frequency signals but also low-frequency signals, with the amplitudes of the high- and low-frequency signals being related by the same coefficients in both channels.

In this case, it was necessary to ensure that the system was configured so that only high frequencies were present in the fast loop control channel, and only low frequencies in the slow loop control channel.

The corresponding changes were made to the system, resulting in more effective suppression of both the low- and high-frequency components of the disturbance spectrum. The effectiveness of this method has also been confirmed by mathematical modeling and corresponding measurements on an experimental setup.

However, the problem of increasing the order of the low-frequency loop remains unresolved. The rationale for increasing the loop order is that, as frequencies decrease, the amplitude–frequency response of the locked loop in the slow-channel range increases more rapidly, with higher loop order in this frequency range. That is, the steeper this characteristic, typically considered on a logarithmic scale, the better. The steepest possible increase in this characteristic within this range is required to improve disturbance–suppression accuracy, enabling the creation of laser and atomic frequency standards with higher accuracy and stability, and reducing the average time required to achieve these characteristics.

Interestingly, second- and third-order control systems have been implemented and used effectively in practice. However, numerical optimization has failed to effectively determine a controller for such systems; the logarithmic amplitude–frequency response method has been used.

However, the numerical optimization method we used, with its developed techniques that include appropriate objective functions, test signals, and some other specific approaches, has proven effective in many problems, including those involving multi-channel systems. However, directly formulating the controller numerical optimization problem for such systems, even with a second-order slow gain loop, has not always been successful, and for higher-order systems, there have been no successful results.

By the order of a loop frequency response in a given frequency range, we mean the order of the slope of the logarithmic amplitude–frequency characteristic in this range.

This paper is devoted to the study of the possibility of calculating a controller for such systems with the second-, third-, and higher-order slow stabilization loops.

2. Statement of the problem

The object has two channels for controlling the output signal. Such objects are known as multiple-input and single-output (MISO) objects.

The equation of an object in the Laplace transform domain is as follows:

$$Y(s) = W_S(s)\,U_1(s) + W_F(s)\,U_2(s) + H(s). \tag{1}$$

Here, all values are given in the form of Laplace transforms of functions of time: $Y(s)$ is the output signal, $U_1(s)$ is the control signal of the slow

channel, $U_2(s)$ is the control signal of the fast channel, $W_S(s)$ is the transfer function of the object's slow channel, $W_F(s)$ is the transfer function of the object fast channel, $H(s)$ is an unknown random disturbance that cannot be measured directly, but it is possible to measure the output value $y(t)$, which corresponds to the signal in operator form $Y(s)$.

The slow channel has a wider control range, sufficient to suppress slow disturbances at expected amplitudes. Therefore, the constraint can be ignored in the slow channel model. The slower response of this channel manifests itself in greater net delay and longer time constants.

Based on these considerations, the transfer function of the slow channel $W_S(s)$ can be defined as follows:

$$W_S(s) = W_1(s)\frac{K_1}{(T_1 s+1)^N}\exp\{-\tau_1 s\} \qquad (2)$$

Here, $W_1(s)$ is the transfer function of the slow channel controller that needs to be calculated, T_1 is the time constant of the slow channel, τ_1 is the time delay in the slow channel, K_1 is the transfer coefficient, s is the argument of the Laplace transform, $N \geq 2$ is an integer exponent.

The transfer function of the fast channel $W_F(s)$ can be defined as follows:

$$W_F(s) = W_2(s)\frac{K_{21}}{T_2 s+1}\exp\{-\tau_2 s\} \qquad (3)$$

Here, $W_2(s)$, is the transfer function of the fast channel controller, which must be calculated, $T_2$is the fast channel time constant, τ_2 is the time delay in the fast channel, K_2 and is the gain. Additionally, the fast channel contains a signal limiter, which is described by the following relationship between the output signal U_{OUT} and the input signal U_{IN}:

$$U_{OUT}(U_{IN}) = \begin{cases} U_{IN}(t), f-a \leq U_{IN}(t) \leq a \\ a, \quad if\ U_{IN}(t) \geq a \\ -a, \quad if\ U_{IN}(t) \leq -a \end{cases} \qquad (4)$$

At the same time:

$$T_1 \gg T_2\ , \tau_1 \gg \tau_2. \qquad (5)$$

The transfer function coefficients K_1 and K_2 are theoretically unimportant for solving the problem, since when optimizing a controller, the required coefficients of the controller must be found, and this result must compensate for an excessively large or excessively small coefficient of the object's transfer function. For example, if this coefficient is increased by the factor M, then all controller coefficients will ultimately decrease by the factor M. However, experience shows that the choice of these coefficients, as well as the selection of starting values for the optimized parameters, can affect the convergence of the optimization procedure and the resulting optimization result if the objective (cost) function has local extrema. This should be considered when solving the controller design problem.

An important feature of the requirements for the designed system should be its ability to suppress low-frequency disturbance, the amplitude of which clearly exceeds the range of achievable maximum amplitude values of the output signal of the fast channel, as well as high-frequency disturbance, the suppression of which is beyond the capabilities of the slow channel.

It is necessary to develop a method for calculating controllers for a system with motion separation, such that the slow channel suppresses low-frequency disturbance, and the fast channel suppresses high-frequency disturbance, while in the region of conjugation of these channels, the slope of the logarithmic amplitude–frequency characteristic of the slow channel corresponds to at least the second order, preferably an even higher order.

The obtained results should be confirmed by numerical simulation, and remain valid after rounding all calculated coefficients to 0.1% (to meet the solution roughness requirement).

A study discusses an empirical method for tuning PID controllers for MISO objects, as well as the application of fuzzy logic. It is acknowledged that, in this case, they were unable to obtain a mathematical formula for the PID controller, nor to create a transparent procedure for tuning the controllers.[20]

In another study, a method of designing controllers using a neural network-based learning procedure is used; no general approach or procedure is developed.[21]

Stefanoiu and Culita[22] used heuristic methods to control a system of two reservoirs, but the stability margin of the resulting MISO system remains uncertain; the reasons are not explained, and the remnants of high-frequency disturbances, as indicated by the resulting transients, are quite large.

In a study by Belmonte *et al.*,[23] the tangential linearization method was used, and no delay links were found in the mathematical models of the object. We do not trust the results of simulations that do not account for delay; such results are usually not confirmed by simulation, except for third- and higher-order objects, which are not included in this article.

Several design strategies are developed:[24] one for first-order MISO systems, providing a flat re-

sponse with a finite settling time, and one for second-order MISO systems, providing a fast response with reduced overshoot and settling time compared to non-hybrid strategies. This study aims to obtain a flat response to a step reference and proposes zeroing the error signal after the output signal reaches the prescribed reference. The effectiveness of this approach is questionable; it is not supported by simulation, and for stabilization systems where the reference is not a jump, but equal to zero, this method is, in any case, inapplicable.

MISO systems are defined as those that simultaneously analyze,[25] for example, both the voltage and current across a load. This approach is unrelated to the motion-dividing method, which uses two drivers with different speeds and dynamic ranges to combine their advantages and eliminate their disadvantages in a single controller.

Reyes-Lúa and Skogestad[26] discuss a method for expanding the output control range by using multiple control channels. The solution consists of connecting the second channel when the output of the first control channel approaches its maximum achievable value, then connecting the third channel according to the same criteria, and so on. This method is used to control multiple pressure-relief valves in a process plant.

3. Method for solving the problem

To solve the problem by using the numerical optimization method during numerical modeling of the system in the VisSim.5.0e software.[27–30] The optimization procedure is built into all versions of VisSim software, including the free demo version. The operating principle of this procedure is described in our article,[28] in Appendix C, which is available in open access.

This requires specifying specific numerical values for all the model's coefficients. Non-zero test signals must also be supplied to the model's input as a task and/or output as a disturbance. A target function must also be used, either a known one or, if necessary, a modified one. It is traditionally recommended to monitor the results using the oscilloscope included with this software, and to read the calculated coefficients from the corresponding final-value indicators (displays).

For controllers, it is recommended to always start with designing PID controllers, i.e., those with proportional, integrating, and derivative channels. The transfer function of such controllers is:

$$W_i(s) = k_{Pi} + \frac{k_{I1}}{s} + k_{Di}\mathrm{s} \tag{6}$$

Here $i = 1$, for a slow channel, $i = 2$ for a fast channel, the coefficients k_{ji} must be calculated using the numerical optimization method.

We typically used stepwise test signals. However, after a series of experiments with varying degrees of success, we concluded that the best approach was to use test signals in the form of harmonic signals at different frequencies, as this is the type of disturbance that the system should effectively suppress. We also tried combining a sum of harmonic signals with different amplitudes and frequencies, as well as a sum of such signals with a stepwise signal. We used all these options in our study.

As an objective function, we usually recommend the cost function, which is so called because it is necessary to find its minimum.[27–30] In this case, the cost function consists of the integral over time from zero to T the sum of at least two different components:

$$F_{Cost}(T) = \int_0^T (\psi_1(t) + w\psi_2(t))\, dt \tag{7}$$

Here is w a weighting coefficient. The developer can set this weighting coefficient at their discretion. More details on the weighting coefficient are provided in Appendix A. The first component, as a rule, was recommended as the product of the error modulus and the time since the start of the transient process. However, since a continuous disturbance is used in this case, unlike the step-suppression problem, zero steady-state error is not important; rather, a small error value throughout the system's operation is sufficient. It is proposed in this case not to use multiplication by the time since the onset of the process, so the first component is proposed simply as the modulus of the control error:[28]

$$\psi_1(t) = |e(t)|. \tag{8}$$

Here $e(t)$ is control error equal to the difference between the output signal prescribed for the system $v(t)$ and its actual signal $y(t)$.

$$e(t) = v(t) - y(t). \tag{9}$$

This same signal $e(t)$ is used for control, as it enters the PID controller's input, and the controller's output is the result of the controller's transformation of this error signal. In this case, two PID controllers are used to control a single output variable.

The second term in **Equation 7** is the result of our previous research; it is equal to the positive part of the product of the error and its deriva-

tive:[29]

$$\psi_2(t) = \max\left\{e(t)\frac{de(t)}{dt},\ 0\right\} =$$

$$= \begin{cases} e(t)\frac{de(t)}{dt},\ if\ e(t)\frac{de(t)}{dt} > 0 \\ 0,\ if\ e(t)\frac{de(t)}{dt} \le 0 \end{cases}. \quad (10)$$

The integral of such a term increases sharply whenever the error signal fluctuates, since the product of the error and its derivative is positive only when the error magnitude increases. Therefore, such a term in the objective function forces the software to search for a controller setting that eliminates or reduces oscillations to a small value. This term also requires a large weighting function, which $w = 1,000$ is typically selected based on the obtained results. If the system experiences excessively large fluctuations or overshoot, this coefficient should be increased further; if the system is excessively slow, this coefficient can be reduced.

Furthermore, we previously concluded that it is useful to use this term to the power of 0.5, that is, to first take its square root. This is justified by the fact that if the system being developed is linear with respect to the input signal, then its performance criteria should also be linearly dependent on the amplitude of the reference signal $v(t)$ and, accordingly, on the amplitude of the error signal $e(t)$.

The stabilization system is formed as follows. The system's output signal, proportional to the laser frequency deviation from the reference cell's clearing frequency, is subtracted from the reference signal, resulting in the system error in accordance with **Equation 9**.

In the domain of Laplace transforms, this equation has the form:

$$E(s) = V(s) - Y(s). \quad (11)$$

Here, the lowercase letters are changed to uppercase, indicating that we are dealing with the Laplace transform, and the argument t is changed from a time to a complex value s.

At the outputs of the controllers, control signals are generated U_i, the equations of the controllers in the Laplace transform domain have the following form:

$$U_i(s) = W_i(s)\,E(s). \quad (12)$$

Each of these signals is fed to the input of the corresponding object channel; the channel's transfer function is defined by **Equations 1** and **2**. The Laplace transform of the output signal is as follows:

$$X(s) = W_S(s)\,U_1(s) + W_F(s)\,U_2(s) =$$

$$= [W_S(s)\,W_1(s) + W_F(s)\,W_2(s)]\,E(s). \quad (13)$$

But the value $X(s)$ describes only the controlled component of the object's output signal. The actual output signal of the object and the system $Y(s)$ also contains the additive component mentioned above, called the disturbance $H(s)$, so an equation describing the addition of this disturbance must be added to this system:

$$Y(s) = X(s) + H(s). \quad (14)$$

Equations 11, 12, 13, and **14** form a system of equations for a closed dynamic system. These equations can be represented by the structural diagram shown in **Figure 2**.

Figure 3 shows the project's block structure in VisSim 5.0e. The hidden part of the of the software VisSim in any version is shown in blue, which means built-in internal algorithm blocks are not indicated in the project picture. The blocks "cost" and "parameter unknown" are the graphically displayed inputs and outputs of these parts of the project. The user can edit the visible parts, and they are displayed in the project. The hidden parts are not edited, but the user can choose one of the three built-in optimization algorithm variants (Appendix C).[28]

4. Theory

According to the structure in **Figure 3**, we have two stabilization loops operating in parallel. The complex Laplace argument s is analogous to frequency. When analyzing locked-loop systems, it is common to use the substitution $s = j\omega$, which converts the Laplace transform into a Fourier transform. The resulting complex transfer function

$$W(j\omega) = W(\omega)\exp\{-j\varphi(\omega)\} \quad (15)$$

describes the dependence of the output signal amplitude gain on the frequency

$$|W(j\omega)| = \sqrt{W(j\omega)\,W(-j\omega)} = W(\omega). \quad (16)$$

and the dependence on the frequency of the phase shift of the signal at the same frequency.

$$\varphi(\omega) = arctg\frac{Im\{W(j\omega)\}}{Re\{W(j\omega)\}}. \quad (17)$$

In the frequency range where

$$|W_S(s)\,W_1(s)| \gg |W_F(s)\,W_2(s)|, \quad (18)$$

there is an approximate relationship

$$X(s) \approx W_S(s)\,W_1(s)\,E(s). \quad (19)$$

In this frequency range, the slow loop operates predominantly.

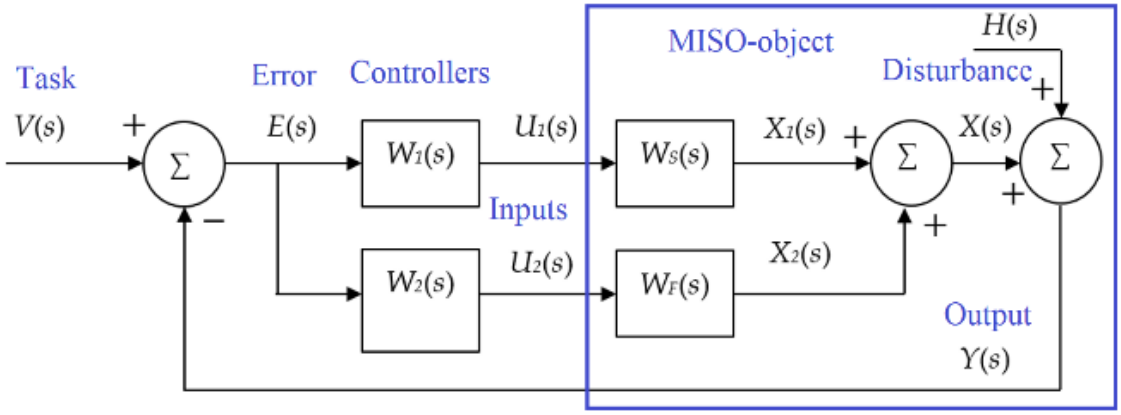

Figure 2. Structure of the laser frequency stabilization system. Abbreviation: MISO: Multiple-input and single-output.

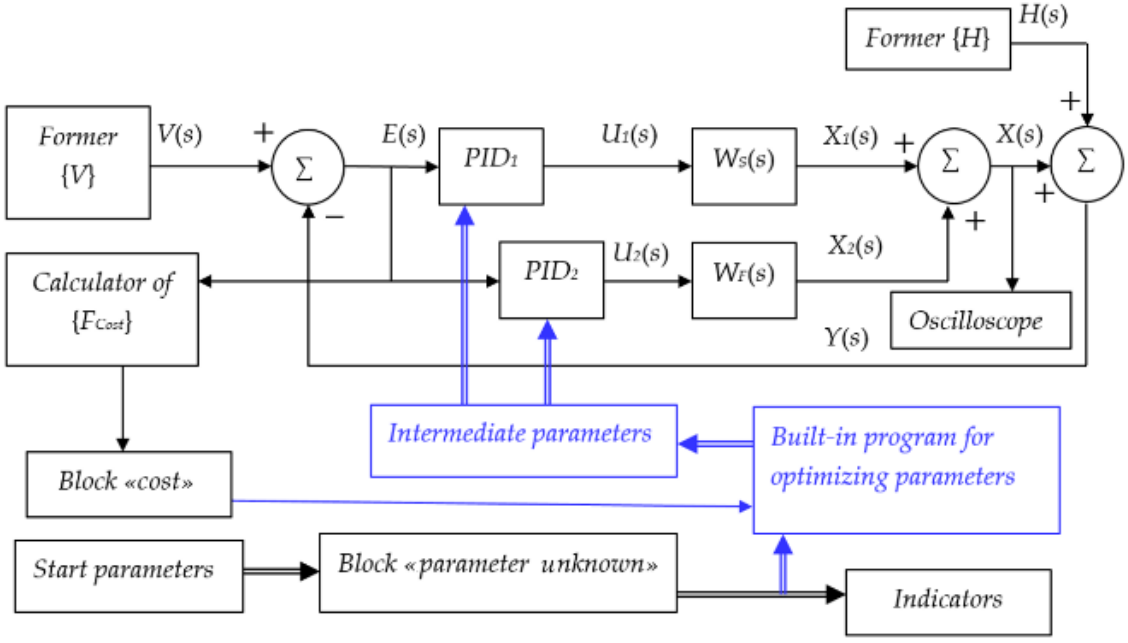

Figure 3. The block structure of the project in VisSim 5.0e.

In the frequency range where

$$|W_S(s)\,W_1(s)| \ll |W_F(s)\,W_2(s)|, \tag{20}$$

there is an approximate relationship

$$X(s) \approx W_F(s)\,W_2(s)\,E(s). \tag{21}$$

In this frequency range, the fast loop operates predominantly.

Where these values are comparable, both loops operate in concert. Consequently, to achieve separate suppression of fast movements by the fast loop and slow movements by the slow loop, it is necessary that relation **(Equation 20)** be satisfied in the region requiring high-frequency suppression, while relation **(Equation 18)** is satisfied in the region requiring low-frequency suppression. To ensure this condition, the graphs of the functions $|W_S(s)\,W_1(s)|$ and $W_F(s)\,W_2(s)$ intersect. Since the slope of these functions on a logarithmic scale depends on the order of the polynomial in the denominator (if the numerator contains only coefficients), it follows that the order of the slow loop must be greater than the order of the fast loop, so that this graph, starting higher in the low-frequency region than the graph of the fast loop, has a greater slope; that is, in the high-frequency region, it takes on smaller values than the graph of the fast loop, as shown in **Figure 4**.

Our assertion that the intersection of the logarithmic amplitude–frequency responses is necessary to ensure the effective operation of both channels is discussed in more detail in Appendix B.

On this basis, the design methodology for such a two-channel controller is clarified as follows. It

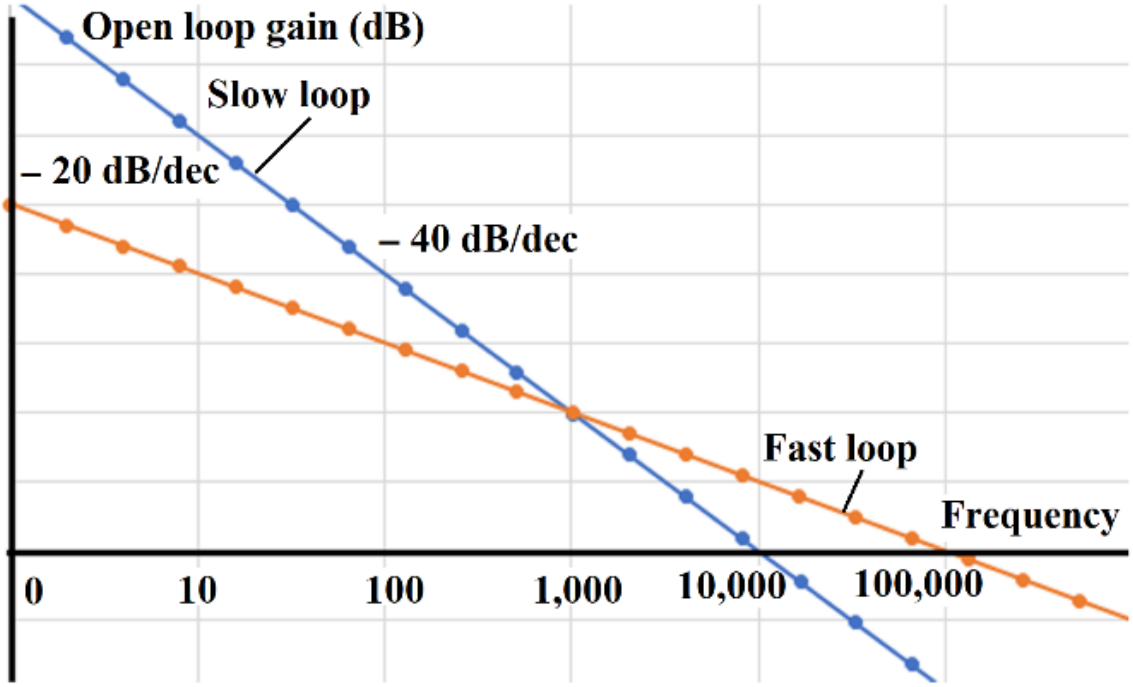

Figure 4. The intersection of the frequency characteristics of the fast and slow loops is possible only under the condition of different slope angles of these characteristics; the characteristic of the slow loop must have a higher slope.

is necessary to ensure that the slow loop has a higher order than the fast loop. Therefore, if the mathematical model of the plant in the slow loop has a higher order than the mathematical model of the fast loop, then each controller can be set to be identical, for example, a PID controller, and then the coefficients of both controllers can be calculated using the numerical optimization method described above. However, in this case, the order of the slow loop can also be further increased by adding a first-order or higher-order filter.

If the mathematical model of the object in both circuits has the same order, then, in addition to the PID controller, a first- or higher-order filter must be added to the slow-loop controller.

5. Results

5.1. Example 1

Let's consider the first variant: the mathematical model of the slow loop has a higher order (second order) than the mathematical model of the fast loop (first order). We define the model of the slow loop in the following form:

$$W_S(s) = \frac{1000}{(100s+1)^2}\exp\{-s\}. \qquad (22)$$

We define the fast loop model as a series connection of a linear part and a limiter, where the transfer function $W_{Ad}(s)$ of the linear part has the following form:

$$W_{S1}(s)\,W_{Ad}(s) = \frac{1}{100s+1} \bullet \frac{1,000}{100s+1}\exp\{-s\}. \qquad (23)$$

We set the output limitation on the fast channel to unity, and the amplitude of the slow disturbance component to five units. In this case, the system cannot suppress such a large disturbance using the fast channel alone, and the slow channel must be used. If such a limitation is not specified, then optimization will seek an optimal solution that eliminates the need for the slow loop.

The structures of PID controllers for each loop are given by **Equation 6**.

Figure 5 shows an overall view of the project in VisSim 5.0e software. Here, the task is a single-step jump. The disturbance is the sum of three harmonic signals, two of which are high-frequency with amplitudes of 0.3 and 0.4 units, and the third is relatively low-frequency with an amplitude of 5 units, while the period of the low-frequency signal is about 320 seconds. In practice, the fast loop operates up to 2 kHz, and the slow loop operates from 0 to 100 Hz. The time scale and, accordingly, the frequency scale can always be recalculated. For modeling, those time and frequency relationships were selected that yield more convenient numerical values of the parameters. In

this project, the following cost function was used

$$F_{Cost}(T) = \int_0^T \left(\psi_1(t) + 100,000\sqrt{\psi_2(t)}\right) dt. \quad (24)$$

This function is derived from **Equation 7** with a weighting factor $w = 100,000$, the second term being taken to the 0.5 power; the reasons for this are explained above. Buses with the same designations are connected in the project, so the signal $v(t)$, which is generated by the fragment in the lower middle part of the figure,

Figure 4 shows that the output signal (blue line) has a single-step shape, indicating it meets the target. However, the signal retains a residual high-frequency disturbance, while the low-frequency disturbance is completely suppressed. The red line shows the disturbance, and the black line shows the system error. The resulting coefficients of the two PID controllers are displayed in the center of the project. The initial values of these coefficients (as constants on the left) differ from the final values; they are taken from the results of previous iterations under different optimization conditions, where the weighting coefficient w in the cost **(Equation 8)** was smaller.

5.2. Example 2

Let us add a first-order filter with a transfer function to the slow loop controller

$$W_{Ad}(s) = \frac{1}{100s+1}. \quad (25)$$

The transfer function of the slow loop controller in this case will have the form

$$W_1(s) = W_{Ad}(s)\left(k_{P1} + \frac{k_{I1}}{s} + k_{D1}\mathrm{s}\right). \quad (26)$$

The mathematical model of the modified slow loop will be the following:

$$W_1 W_S(s) = \left(k_{P1} + \frac{k_{I1}}{s} + k_{D1}\mathrm{s}\right) \times \frac{1,000}{(100s+1)^3}\exp\{-s\}. \quad (27)$$

All other conditions are the same as in Example 1. In particular, the transfer function of the fast channel together with the controller has the form:

$$W_F(s) = \left(k_{P2} + \frac{k_{I2}}{s} + k_{D2}\mathrm{s}\right)\frac{10}{10s+1}\exp\{-0.1s\}. \quad (28)$$

Figure 6 shows the result of solving this problem using the same method. Residual high-frequency deviation is also present in the output signal.

As a rule, previous studies did not include the delay link in the fast and slow channels of the object models, considering it negligible. We included it in the model because we believe that a model without a delay link is incomplete. However, the delay value was chosen without any particular justification. Therefore, additional modeling was undertaken with a smaller delay link in the fast channel.

5.3. Example 3

With the same conditions as in Example 2, we take the delay in the fast channel is to be five times smaller:

$$W_F(s) = \frac{10}{10s+1}\exp\{-0.02s\}. \quad (29)$$

The transfer function of the slow loop with a controller is given by **Equation 27**. The transfer function of the fast loop is given by the equation:

$$W_F(s) = \left(k_{P2} + \frac{k_{I2}}{s} + k_{D2}\mathrm{s}\right)\frac{10}{10s+1}\exp\{-0.02s\}. \quad (30)$$

The same solution method with the same conditions yields the result shown in **Figure 5**. We rounded the controller coefficient calculation results to three significant digits, then disabled the "run optimization" option and repeated the simulation using the "track memory" function. The mathematical simulation showed that, after rounding, the system's transient processes changed insignificantly, and the resulting deviations did not exceed the line width. This allows us to conclude that the obtained result is robust, as required by the problem conditions. To illustrate how this system operates, **Figure 7** shows the signals at the outputs of the fast and slow loops separately. The red trace is the output of the slow loop, containing only low frequencies. The black trace is the output of the fast loop, containing only high frequencies. The blue signal is the system output, and since the setpoint in this project is zero, it represents the system error. The error is essentially zero or very close to zero, with no residual high-frequency deviation.

It remains an important theoretical and practical task to develop a design methodology for such a two-channel controller for the case where the order of the slow circuit exceeds three.

As the order of this loop increases, the difficulty of optimization is so sophisticated that the attempt to do it it often fails. This manifests when some values reach an unacceptable absolute magnitude, exceeding 10^{28}. Typically, such a value is a signal in the system, and the result arises from significant instability of the obtained intermediate solution.

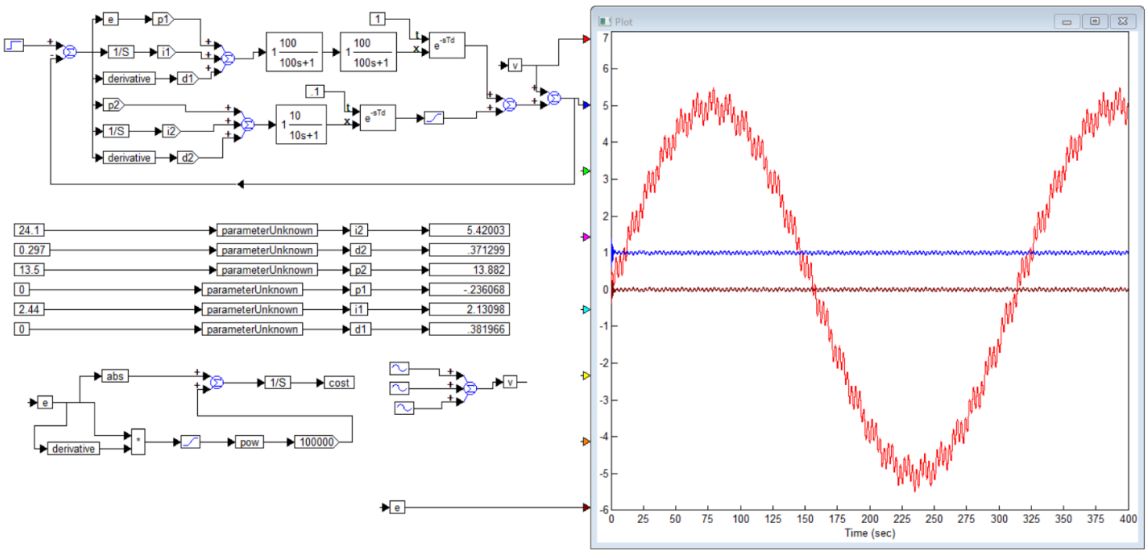

Figure 5. General view of the **Example 1** project in VisSim 5.0e software ($n = 2$).

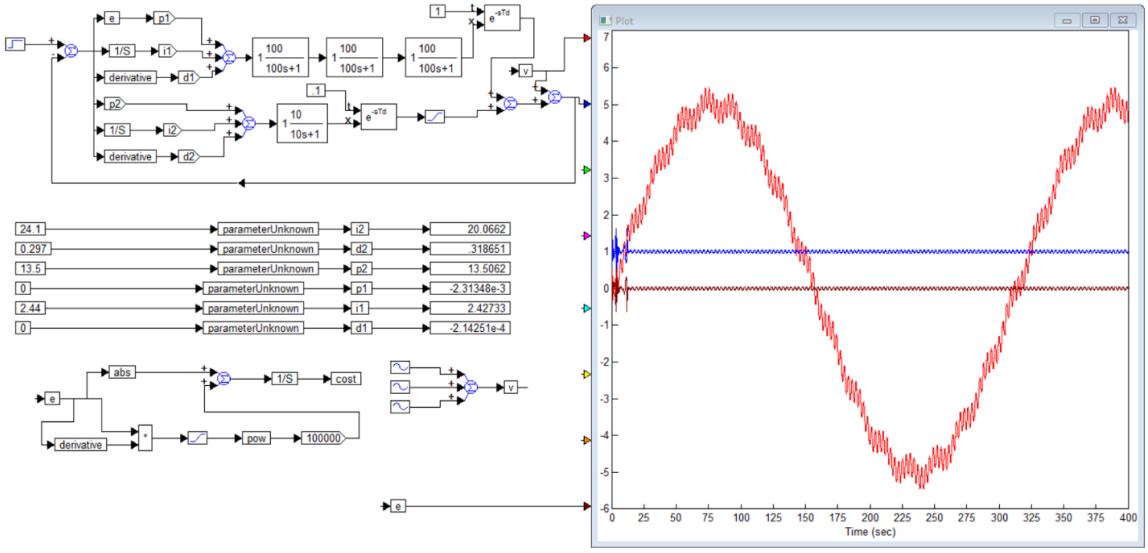

Figure 6. General view of the **Example 2** project in the VisSim 5.0e software ($n = 3$).

In this case, the optimization is interrupted, the corresponding block whose output value is outside the allocated range is colored red, and a message is issued stating that the optimization operation could not be completed.

One possible solution to this problem is to transform global search into local search. To do this, the cost function should include terms that increase significantly as any optimized parameter approaches the undesirable value for it. However, since the undesirable range of values is unknown in advance, this approach can be very time-consuming and require an inordinate number of optimization runs.

We have proposed and successfully tested another method. It consists of initially setting all the coefficients of the slow loop to zero and not participating in the optimization procedure. That is, the initial values of this loop from the zero constant output are fed to the coefficient control input of this controller, bypassing the "parameter unknown" blocks. During optimization, the disturbance signal consists only of high-frequency components, the sum of which never exceeds the set limiting threshold at the fast channel output, or a stepwise jump in the reference or disturbance can be used, the magnitude of which does not exceed 50% of the limiting value at the fast loop output. In this case, the slow channel is not required, and the software tool effectively finds the fast-channel controller coefficients. In the second stage, these coefficients are fixed and are not subject to optimization. In this case, the disturbance signal is a slow harmonic signal with an amplitude that is a multiple of the fast channel limiting level. Under these conditions, the numerical optimiza-

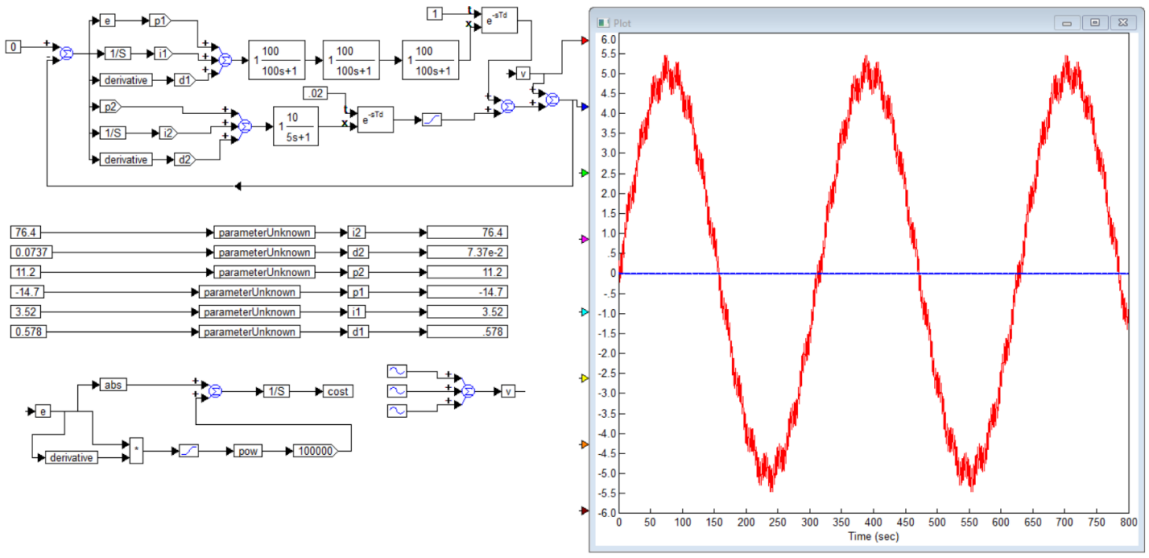

Figure 7. General view of the **Example 3** project in the $N = 3$.VisSim 5.0 e software.

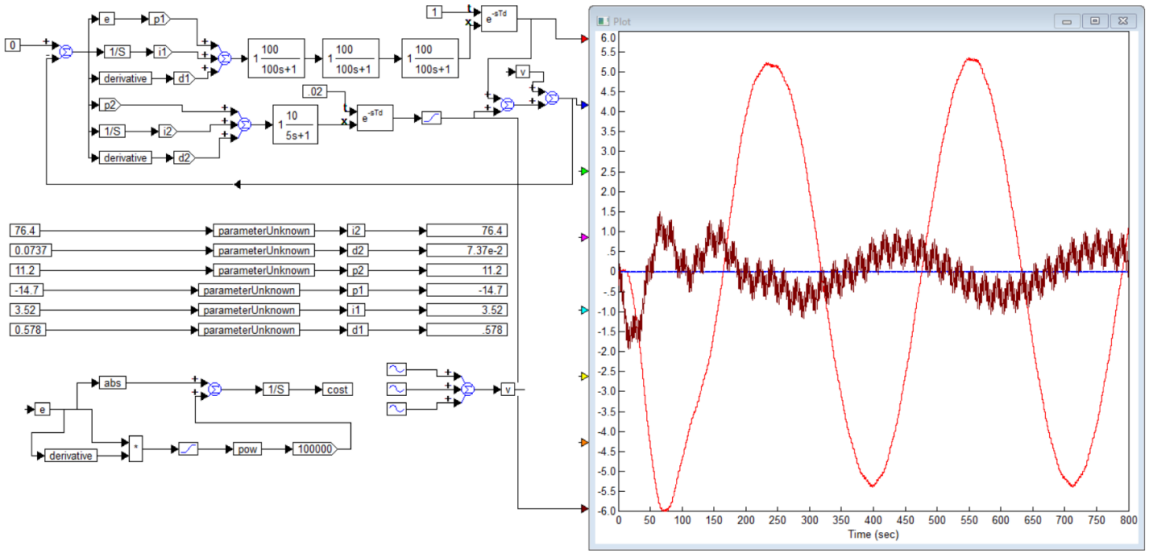

Figure 8. The same system: the output signals of the slow loop (red line) and the fast loop (black line), as well as the output signal of the system, equal to the sum of the disturbance and the output signals of the two control loops, together, the two loops completely suppress the disturbance.

tion procedure is restarted, this time to calculate the slow loop coefficients.

In this way, all six coefficients of the two-channel controller are determined: three coefficients for the fast-loop PID controller and three coefficients for the slow-loop PID controller.

A third stage was also tested, in which all the found coefficients of both controllers were set as new starting values, after which the numerical optimization procedure was run again. In this case, the disturbance signal contained all previously used components, i.e., one or more high-frequency disturbance components, collectively not exceeding the fast-loop threshold, and a slow harmonic signal, a multiple of this threshold. In this case, the optimization procedure was successful and allowed us to find a new solution that was slightly better than the starting set of coefficients in terms of smaller high-frequency error components.

It should be noted that the high order of the slow loop is achieved not only by the properties of the piezoelectric modulator, but primarily by the implementation of a corresponding dynamic element in the electronic control module, either analog or digital. Of course, the slow-loop modulator itself is a second-order object, and the higher order is achieved by the electronic filter, which functions as a correction device. The higher the order of this filter, the slower its response time, provided the time constants of this loop remain the same. Therefore, as the order of this filter increases, its time constant should be reduced to

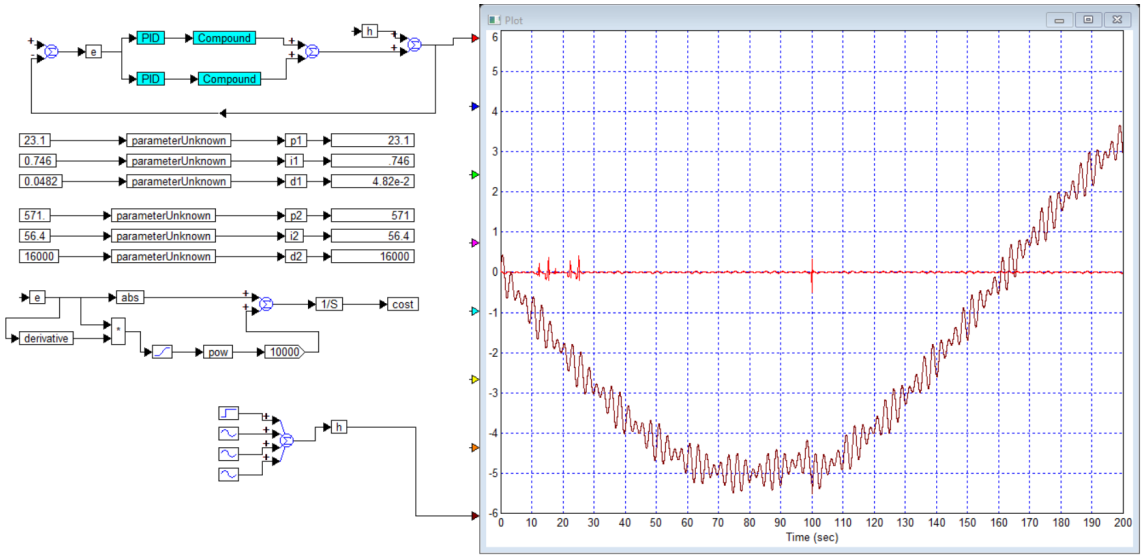

Figure 9. Result of step-by-step optimization of the system of **Example 4**: the signal $y(t)$ at the output of the system as a whole (red line) and the disturbance $h(t)$ applied at the output of the object (black line).

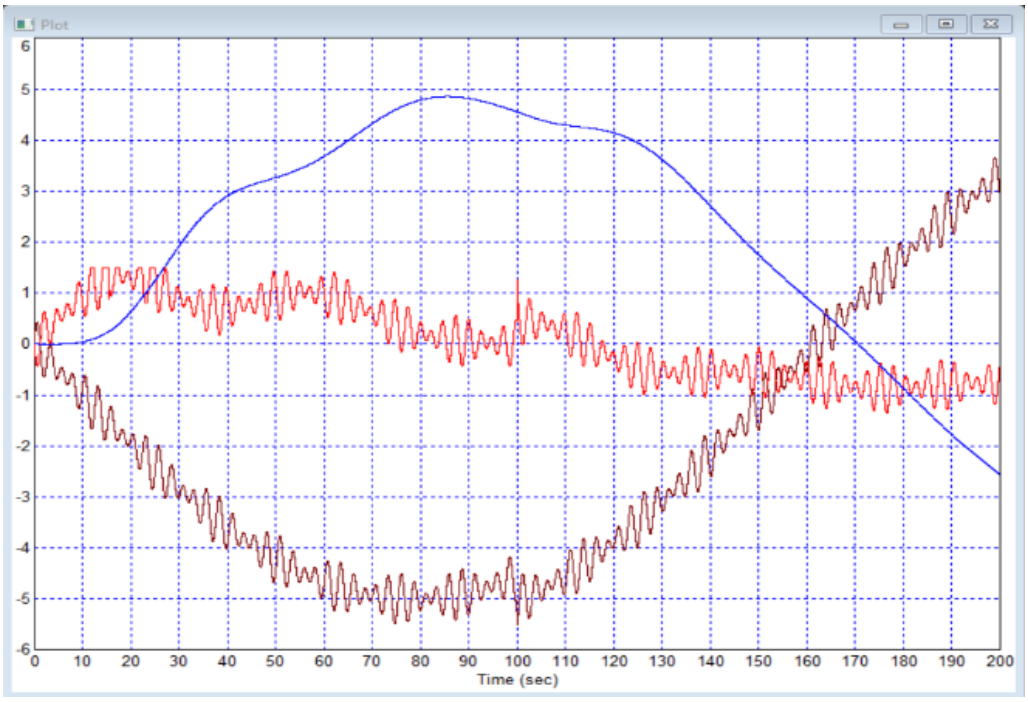

Figure 10. Signals in the system, according to **Figure 7**: blue line – output signal of the slow channel $x_1(t)$, red line – output signal of the slow channel $x_1(t)$, black line – total disturbance $h(t)$.

achieve the desired improvement in disturbance suppression.

5.4. Example 4

Let us define a slow loop model together with an additional filter in the following form:

$$W_S(s)\,W_{Ad}(s) = \frac{1}{(10s+1)^5}\exp\{-s\}. \qquad (31)$$

We define the fast loop model as a series connection of a linear part and a limiter, where the transfer function of the linear part has the following form:

$$W_F(s) = \frac{10}{5s+1}\exp\{-0.02s\}. \qquad (32)$$

Also, the fast loop still has a limiter at its output.

Based on the results of the first iteration step, we obtained the following coefficients for the fast-loop PID controller: k_{P2}= 23.0865, k_{I2}= 0.745965, k_{D2}= 0.0482396. After rounding, we obtain the transfer function of the fast con-

troller:

$$W_2(s) = 23.1 + \frac{0.746}{s} + 0.0482\text{s}. \qquad (33)$$

By fixing these coefficients in the second procedure, we obtain the following coefficients for the slow-loop PID controller: $k_{P1} = 571.046$, $k_{I1} = 56.3617$, $k_{D1} = 16,001.1$. After rounding, we obtain the transfer function of the fast controller:

$$W_1(s) = 571 + \frac{56.4}{s} + 16,000\text{s}. \qquad (34)$$

Figure **Figure 8** shows the slow and fast channel signals separately in the same system shown in Figure **Figure 7**. **Figure 9** shows the design and the result of step-by-step optimization of the Example 4 system: the signal $y(t)$ at the output of the system as a whole (red line) is close to zero, but there are individual spike-shaped disturbances, the disturbance $h(t)$ coming to the output of the object (black line) is almost completely suppressed by two feedback loops in the system.

Figure 10 shows the slow channel output signal separately $x_1(t)$ (blue line), the slow channel output signal $x_1(t)$ (red line), and for comparison, the disturbance $h(t)$ (black line).

The final stage with numerical optimization of all six coefficients from the obtained starting value does not provide significant improvements.

Simulations with different frequencies for the slow and fast disturbance components confirmed that these two loops successfully suppress disturbances within their respective frequency ranges. Thus, the stated problem has been solved.

6. Discussion

The use of a fifth-order filter in the stabilization circuit may come as a big surprise to control theory specialists.

The Nyquist-Mikhailov stability criterion for the logarithmic amplitude-frequency response of an open-loop system with negative feedback is well known. It states that the phase–frequency response of this circuit $\varphi(\omega)$ should not cross the lower limit of its value $\varphi(\omega) = -\pi$ within the frequencies where the logarithmic amplitude–frequency response remains positive. A fifth-order filter brings the phase–frequency response of this circuit $\varphi(\omega)$ to a value $\varphi(\omega_r) = -2.5\pi$, where the argument ω_r denotes the frequencies at which the slope of the amplitude–frequency response is approximately -100 dB/dec. However, this criterion is not violated here, since its requirement allows the phase response to exceed this limit, provided that as the frequency increases, while the amplitude–frequency response of the open-loop remains positive, this phase-frequency response will have time to return to the limits designated by this demand. If such a characteristic is represented as a hodograph of the corresponding vector, marking the values of the complex transfer function, where the phase delay of this function at a given frequency is displayed by the rotation angle of the vector, and the gain at this frequency is the length of the vector. Then such a hodograph, when the frequency changes from zero to infinity, starting on the real axis, will make a revolution around the center of coordinates, sequentially passing through four quadrants and then back to the initial quadrant, after which it will return to the second quadrant even before its amplitude is less than one, so that such a hodograph formally does not cover the point with coordinates $\{-1, j0\}$.

7. Conclusion

A fundamentally new result of this article is the idea that it is preferable to increase the order of the slow loop to third or higher. Our previous studies[19–23] showed that the fast loop should be first, while the slow loop should be second or higher, but an order higher than second has not been investigated by numerical simulation and has previously been justified only in general terms. In this paper, the feasibility and effectiveness of this solution are demonstrated through simulation.

The disturbance suppression coefficient can be estimated, for example, based on the results of Example 3. The residual deviations of the output signal in the stabilization system do not exceed the line width in **Figure 9**, i.e., their amplitude is no more than $\pm$ 0.025 *units* over the entire frequency band. The slow disturbance fed to the object output via the adder has an amplitude $\pm$ 5 units at a frequency with a period of approximately 320 s. Consequently, at this frequency, disturbance suppression is ensured by at least 200 times. Moreover, the amplitude of the slow disturbance is greater than the maximum output signal of the fast loop, limited by $\pm$ 1 units. Also, separate consideration of the output signals of the slow and fast circuits demonstrates that the separation of functions and movements in these channels is successfully achieved. The amplitude of the fast disturbance is approximately $\pm$ 0.25 units, i.e., the fast disturbance is suppressed by at least 10 times. Moreover, the fast component is formed from the sum of harmonic signals with periods of approximately 20 seconds and approximately 2 seconds. In addition to suppressing fast disturbances, the fast channel ensures the stability of

the entire system; if it is disabled, the system becomes unstable. In existing full-scale prototypes of such a system, experiments have shown that the system remains stable when the fast channel is disabled. This can only occur if the amplitude–frequency response curves of the fast and slow channels are parallel, meaning they do not intersect, as required for the effective operation of both loops. Following these studies, modifications were recommended and implemented to these systems, ensuring deeper disturbance suppression due to the effective operation of both loops, something previously unheard of. The results of this paper provide the basis for further refinement of such systems, ensuring a steeper slope of the slow-loop amplitude–frequency response in the low-frequency region, thereby increasing the rise of this characteristic with decreasing frequency, and increasing the depth of disturbance suppression at low frequencies.

The effect of limiting in the fast loop manifests as insufficient system performance when the fast channel's output signal reaches the limiting threshold. Since the magnitude of high-frequency disturbance in laser systems is known and is generated by acoustic noise, the limiting level, according to calculations, is twice the minimum required to suppress this disturbance. To ensure that limiting the fast channel's output signal does not affect system operation, it is necessary and sufficient to ensure that the fast loop does not produce a large response signal to large low-frequency inputs. Thus, if the problem of frequency separation into two loops is successfully solved, then the limiting problem is also automatically solved. The purpose of frequency separation into two loops is precisely to eliminate responses to slow, large components of the disturbance signal from the fast loop. On the other hand, since the problem of fast-loop limitation has been effectively solved, this allows the use of an amplifier with a lower output signal amplitude. This allows the output impedance of the amplifier in this channel to be reduced and therefore broaden the gain bandwidth of the fast loop and, consequently, to expand the entire band of the system, since one of the factors limiting the frequency band of the laser radiation stabilization system was the impossibility of implementing a high-voltage amplifier with a low output impedance, or this required additional unjustified energy costs and caused overheating of the amplifier. For example, a signal amplitude of 300 volts with an amplifier output impedance of 50 ohms assumes excessively large currents of this amplifier, whereas with an amplitude of 10 volts, such an output impedance is much easier to provide; the power required is 900 times less (since the power at a fixed resistance depends on the voltage according to a square law).

Acknowledgments

None.

Funding

This work was accomplished by the Center of Competence for Mechatronics and Clean Technologies "Mechatronics, Innovation, Robotics, Automation and Clean Technologies"–MIRACle, with the financial support of contract no. BG16RFPR002-1.014-0019-C01, funded by the European Regional Development Fund (ERDF) through the Program "Research, Innovation and Digitalization for Smart Transformation" (PRIDST) 2021–2027.

Conflict of interest

The authors declare that they have no conflict of interest in the publication of this article.

Availability of data

Conceptualization: All authors
Investigation: Lubomir Dimitrov
Methodology: Vadim Zhmud
Formal analysis: Vadim Zhmud
Writing – original draft: All authors
Writing – review & editing: Lubomir Dimitrov

AI tools statement

All authors confirm that no artificial intelligence tools were used in the preparation of this manuscript.

References

1. Wu Y, Qin F, Li Y, Ding Z, Xu R. Designing an Automatic Frequency Stabilization System for an External Cavity Diode Laser Using a Data Acquisition Card in the LabVIEW Platform. *Appl. Sci.* 2024;14:308. https://www.doi.org/10.3390/app14010308
2. Petrenko MV, Pazgalev AS, Vershovskii AK. Method of Laser Frequency Stabilization Based on the Effect of Linear Dichroism in Alkali Metal Vapors in a Modulated Transverse Magnetic Field. *Photonics.* 2024;11:926. https://www.doi.org/10.3390/photonics11100926
3. Jin K, Geng X, Liang Z, *et al*. Design of Portable Self-Oscillating VCSEL-Pumped Cesium Atomic Magnetometer. *Electronics.* 2022;11:3666.

https://www.doi.org/10.3390/electronics11223666
4. Singh V, Tiwari VB, Mishra SR, Rawat HS. A tunable Doppler-free dichroic lock for laser frequency stabilization. *Appl Phys B.* 2016;122(225). https://www.doi.org/10.1007/s00340-016-6497-6
5. Zhao W, Zhou X, Shang J, *et al*. Synchronous achievement of laser frequency stabilization and tunability via modulation transfer spectroscopy on the rubidium D1 line. *Opt Commun.* 2024;574. https://www.doi.org/10.1016/j.optcom.2024.131153
6. Jeong J, Lee S, Hwang S, Baek J, Noh,HR, Moon G. Theoretical and Experimental Study of Optimization of Polarization Spectroscopy for the D2 Closed Transition Line of 87Rb Atoms. *Appl Sci.* 2021;11(16):7219. https://www.doi.org/10.3390/app11167219
7. Beica HC, Winter S, Mok C, Barrett B, Berthiaume R, Vorozcovs A, *et al*. Laboratory Courses on Laser Spectroscopy and Atom Trapping. *Atoms.* 2020;8(2):25. https://www.doi.org/10.3390/atoms8020025
8. Kim J, Kim K, Lee D, *et al*. Locking Multi-Laser Frequencies to a Precision Wavelength Meter: Application to Cold Atoms. *Sensors.* 2021;21: 6255. https://www.doi.org/10.3390/s21186255
9. Wang J, Gao Y, Yu J, *et al*. Multi-Wavelength Narrow-Spacing Laser Frequency Stabilization Technology Based on Fabry -Perot Etalon. *Micromachines.* 2024;15:1269. https://www.doi.org/10.3390/mi15101269
10. Liu C, Yue Z, Xu Z, Ding M, Zhai Y. Far Off-Resonance Laser Frequency Stabilization *Technology. Appl. Sci.* 2020;10:3255. https://www.doi.org/10.3390/app10093255
11. Bengalskii D, Kharasov D, Fomiryakov E, Nikitin S, Nanii O, Treshchikov V. (2023). Characterization of Laser Frequency Stability by Using Phase-Sensitive Optical Time-Domain Reflectometry. *Photonics.* 2023;10:1234. https://www.doi.org/10.3390/photonics10111234
12. Wu Y, Qin F, Ding Z, Xu R, Li D. Research on the Frequency Stabilization System of an External Cavity Diode Laser Based on Rubidium Atomic Modulation Transfer Spectroscopy Technology. *Photonics.* 2024;11:298. https://www.doi.org/10.3390/photonics11040298
13. Fan L, Jiao D, Liu J, *et al*. Prompt Frequency Stabilization of Ultra-Stable Laser via Improved Mean Shift Algorithm. *Electronics.* 2022;11; 1319. https://www.doi.org/10.3390/electronics11091319
14. Ming Z, Li X, Wang Y, *et al*. Compact High-Precision Cascade PID-Control Laser Driver for Airborne Coherent LiDAR Applications. *Sensors.* 2025;25:2851. https://www.doi.org/10.3390/s25092851
15. Wei Y, Wang Z, Wang Y, *et al*. Red-Pitaya-Based Frequency Stabilization of 1560-nm Fiber Laser to 780-nm Rubidium Atomic Transition via Single-Pass Frequency Doubling. *Photonics.* 2026;13:57. https://www.doi.org/10.3390/photonics13010057
16. Bagaev S, Vasilenko L, Goldort V, Dmitriev A, and Dychkov S. (1977). Helium - neon laser emitting $\lambda = 3.39$ μ line of 7 Hz width. *Sov J Quantum Electron.* 1977;7(5):665-666. https://www.doi.org/10.1070/QE1977v007n05ABEH012784
17. Bagayev SN, Belkin AM, Dychkov AS, *et al*. Frequency reference in the 732-nm region for precision laser spectroscopy of muonium. *Quantum Electronics.* 2000;30(7):641-646. https://www.doi.org/10.1070/QE2000v030n07ABEH001782
18. Zhuang S, Li J, Wang H, Deng J, Mao Y. Multi-Channel Phase-Compensated Active Disturbance Rejection Control with an Improved Backstepping Strategy for Electro-Optical Tracking Systems. *Actuators.* 2024;13:117. https://www.doi.org/10.3390/act13030117
19. Zhmud VA. New approaches to controlling the frequency of laser light. In: *AIP Conference Proceedings.* 2019;20981):020020. https://www.doi.org/10.1063/1.5098164
20. Sałabun W, Wieckowski J, Shekhovtsov A, Palczewski K, Jaszczak S, Wątróbski J. How to Apply Fuzzy MISO PID in the Industry? An Empirical Study Case on Simulation of Crane Relocating Containers. *Electronics.* 2020;9:2017. https://www.doi.org/10.3390/electronics9122017
21. Ramos-Martinez M, Brizuela -Mendoza JA, Torres- Cantero CA, *et al*. Implementation of an Intelligent Controller Based on Neural Networks for the Simulation of Pressure Swing Adsorption Systems. *Algorithms.* 2025;18:215. https://www.doi.org/10.3390/a18040215
22. Stefanoiu D, Culita J. Optimal Identification and Metaheuristic PID Control of a Two-Tank System. *Electronics.* 2021;10:1101. https://www.doi.org/10.3390/electronics10091101
23. Belmonte LM, Segura E, Fernández -Caballero A, Somolinos JA, Morales R. Generalized Proportional Integral Control for Magnetic Levitation Systems Using a Tangent Linearization Approach. *Mathematics.* 2021;9:1424. https://www.doi.org/10.3390/math9121424
24. Sáez JF, Baños A. Reset Control of Parallel MISO Systems. *Mathematics.* 2021;9:1823. https://www.doi.org/10.3390/math9151823
25. Dyga L, Alhasheem M, Davari P, Rymarski Z. Robustness of Model-Predictive and Passivity-Based Control in the Three-Phase DC/AC Converter Application. *Appl Sci.* 2022;12:4329. https://www.doi.org/10.3390/app12094329
26. Reyes-Lúa A, Skogestad S. Multiple-Input Single-Output Control for Extending the Steady-State Operating Range—Use of Controllers with Different Setpoints. *Processes.* 2019;7:941. https://www.doi.org/10.3390/pr7120941
27. Zhmud VA, Dimitrov LV. The influence of the type of the test signal on the result of numeri-

cal optimization of regulators. *J Phys: Conf Ser.* 2017;803:012186. https://www.doi.org/10.1088/1742-6596/803/1/012186
28. Zhmud V. Controlling of Multichannel Objects with Non-Square Transfer Function. *Automation.* 2025;6:27. https://www.doi.org/10.3390/automation6030027
29. Zhmud V, Dimitrov L. Control of Linear Multichannel Objects with Numerical Optimization. *Appl. Sci.* 2025;15(16):8927. https://www.doi.org/10.3390/app15168927.
30. Zhmud VA, Nosek J, Dimitrov LV, Boyarchikov EYu. Nonlinear PID Controller for Effective Suppression of Oscillations When Controlling an Oscillating Object with a Delay. In: *Smart Innovation, Systems and Technologies.* Springer Nature Singapore; 2022:175-182. https://www.doi.org/10.1007/978-981-16-8759-4_19

Vadim Zhmud *ia s leading recearcher in Institute of Laser Physics of the Siberian Branch of the Russian Academy of Sciences, and in Department of Monitoring of Crustal Deformations, Altai-Sayan branch of the Federal State Budgetary Institution of Science Geophysical Service of the Russian Academy of Sciences, Novosibirsk, Russia. Professor of Novosibirsk State University. Doctor of Technical Sciences, member of Expert Council of the Higher Attestation Commission of Russia. Interest sphere: laser physics, photonics, control systems, modelling, optimization, electronics control systems, ADC, DAC.*
https://orcid.org/0000-0002-1708-9211

Lubomir Dimitrov, *Professor in the field of "Mechanical engineering and Mechatronics" at the Technical University of Sofia, Bulgaria. Graduated from Moscow Technological University, Russia (1980). Specialized at Cambridge University, UK, University of Cincinnati, USA, Dublin University, Ireland. Author of many publications in this field of Mechanical engineering and Mechatronics.*
https://orcid.org/0000-0001-8584-5958

Appendix A. Application of the weighting factor in the cost function

Applying a weighting factor to the cost function ***(Equation 7)*** *shifts the emphasis of the resulting system's requirements from one indicator to another. For example, if this weighting function is small,* $w < 100$*, then, as a rule, the second term in* ***Equation 7*** *has virtually no effect on the overall sum. Therefore, such a function does not force the optimization algorithm to search for controller coefficient values that keep this term small. In this case, the transient process retains significant overshoot and large oscillations. If this factor is made very large, for example,* $w > 10,000$*, then the second term will make a very large contribution to the cost function* ***(Equation 7)****. In this case, the optimization algorithm will seek controller coefficient values that eliminate overshoot and oscillations. However, the relative contribution of the first term to the cost function will decrease, and, consequently, the optimization algorithm will not strive to find controller coefficient values that ensure the most rapid termination of the transient process. By selecting a weighting function value in the range,* $100 > w > 10,000$*, the system designer can choose between reducing the transient response time and eliminating oscillations and overshoot. Typically, a compromise solution lies somewhere in the middle. In* ***Equation 7****, only one weighting function is used, applied to only one of the two terms. A weighting function with the first term is not required, since the algorithm seeks controller coefficient values at which the value* $F_{Cost}(T)$ *from* ***Equation 7*** *is minimized. Therefore, if two weighting factors were used, the result would be the same as dividing this value by the first weighting factor. Therefore, in this relationship, we can set one of the weighting factors equal to one. Therefore, the designer should first specify a weighting factor, evaluate the result, and then adjust it to achieve the desired system properties. This is always a compromise: given the properties of the mathematical model, increasing performance beyond a certain point causes the system to overshoot and oscillate, and reducing overshoot and oscillation can be achieved at the cost of reducing the performance.* ***Figure A1*** *shows different results of controller optimization for different values of the weighting coefficient in the cost function* ***(Equation 7)*** *for an object whose model is given by a transfer function of the form* ***(Equation 23)*** *from Example 1.*

Figure A2 *shows different results of controller optimization for different values of the weighting coefficient in the cost function* ***(Equation 7)*** *for an object whose model is given by the following transfer function:*

$$W(s) = \frac{10}{10s^2 + 0.1s + 1}\exp\{-0.5s\}. \qquad (35)$$

Thus, the choice of the weighting function allows the designer to prioritize one of two requirements: (i) high response speed; (ii) low overshoot and oscillation, or even their complete absence. In practice, it is sufficient to evaluate the resulting transient response. If the designer believes that oscillations and overshoot should be better suppressed, at the cost of some loss in performance, then the coefficient w *should be increased until the desired result is achieved. If this fails, a different, more complex controller should be used, for example, one containing an additional channel with double derivation.*

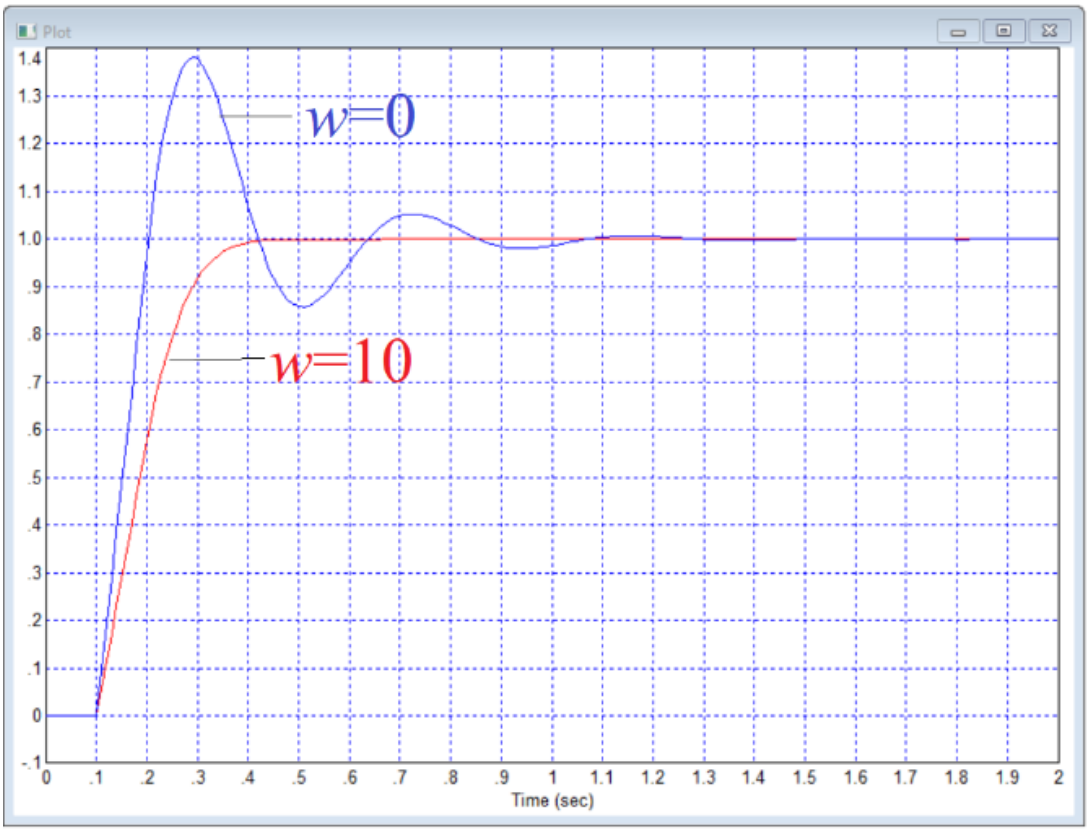

Figure A1. Different results of controller optimization for the different values of the weighting coefficient in **Equation 7** for object **(Equation 23)** from Example 1: the blue line is the transient process in the system with a controller calculated according to **(Equation 7)** at $w = 0$, the red line is the transient process in the system with a controller calculated according to **(Equation 7)** with $w = 10$.

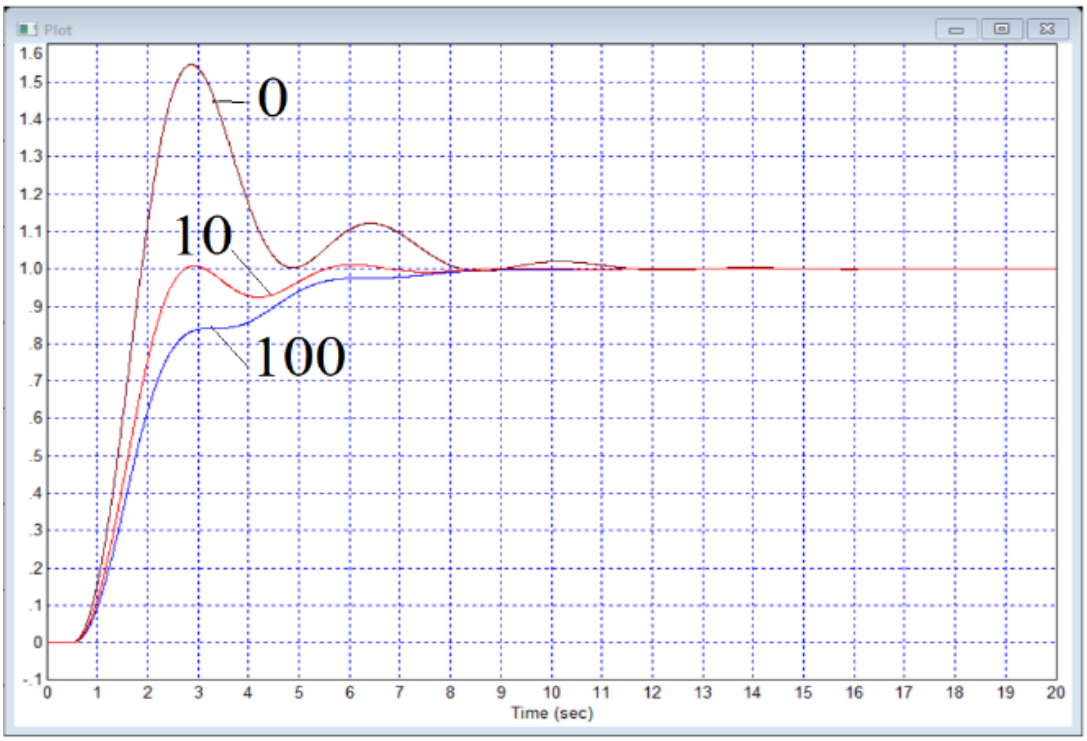

Figure A2. Different results of controller optimization for different values of the weighting coefficient in **Equation 7** for object **(Equation 35)**; the values of the weighting function are indicated next to the corresponding transient process curves.

Appendix B

The assertion that the logarithmic frequency responses of the slow and fast loops are valid is supported by the fact that in the low-frequency range, the slow loop's transfer function must be larger, while in the high-frequency range, the fast loop's transfer function must be larger. To satisfy this condition, these transfer functions must intersect. Typically, the slope of such functions on a logarithmic scale depends on those factors that change significantly with increasing frequency in this frequency range, while the remaining factors, which change insignificantly with increasing frequency in this frequency range, do not significantly contribute to the slope of this characteristic. In this sense, one can say that the slope of the frequency response varies across different sections, but such sections can be relatively extended. This is the basis for the well-known method of constructing such characteristics using their asymptotes.

For example, consider four transfer functions

$$W_{11}(s)=\frac{k}{s}, W_{12}(s)=\frac{k}{s(1+s)},$$

$$W_{13}(s)=\frac{k(1+0.01s)}{s(1+s)},$$

$$W_{14}(s)=\frac{k(1+0.01s)}{s(1+s)(1+0.0001s)}. \quad (36)$$

In the frequency domain, $\omega \ll 1$, it can be argued that $s \ll 1$, therefore, all these four transfer functions are approximately equal, so that in this frequency domain, the graphs of all these functions $W_{1k}(\omega)$ at $s=j\omega$ have the same appearance, since $1+s\approx 1$, and $1+0.01s\approx 1$ also $1+0.0001s\approx 1$, and all of these graphs have a slope -20db/dec that is, within this frequency range, all of these transfer functions behave like integrators. This is shown in ***Figure B1****. In the frequency range where $0.2<\omega<20$ the factor $(1+s)$ in the denominator of the last three transfer functions, a value that differs significantly from unity is acquired, and the higher the frequency, the smaller the contribution to this factor is made by the term equal to unity. For this reason, in this frequency range, the last three transfer functions have a slope of -40 db/dec, while the first transfer function does not change its previous slope. Further, with increasing frequency, in the region where $20<\omega<2,000$ the factor $(1+0.01s)$ in the numerator of the last two transfer functions, also begins to differ significantly from unity, as a result of which, in this frequency range, the slope of these two transfer functions changes as if in the denominator there was s^2, and in the numerator, a factor appeared s, so that these two transfer functions are approximately similar to an integrator, and they will again have a slope in this frequency range -20 db/dec. Finally, in the frequency range where $2,000<\omega$, the final transfer function also begins to show the influence of the factor $(1+0.0001s)$, in which the second term will be significantly greater than unity with increasing frequency. So, in this frequency range, the final transfer function will behave like a second-order link, that is, like two integrators connected in series. In this sense, we can say that in different frequency ranges, transfer functions can behave like filters of different orders. This slope determines the phase delay at these frequencies. The system will be stable only if its logarithmic frequency response intersects the frequency axis with a slope no greater than second order; that is, it must be a first-order slope or a fractional slope in the interval between first and second orders. The closer the slope to the second-order slope, the smaller the system's stability margin. Therefore, a first-order slope is preferable. This information is widely known in the literature on automatic control theory. Therefore, for the fast loop, the preferred choice remains a first-order slope. Since the logarithmic amplitude–frequency response of the slow loop must intersect it, a slope of at least second order is recommended. In our article, we use numerical simulation methods for the first time to explore the possibility of implementing a slope higher than second order for the slow loop.*

The requirement for one of the many circuits to dominate is a requirement for a greater absolute value of the transfer function of that circuit in that frequency range. The disturbance suppression coefficient at a fixed frequency ω_1 is equal to the coefficient of the entire circuit, that is, the absolute value of

$$W(\omega_1)=$$

$$\sqrt{|W_S(\omega_1)W_1(\omega_1)|^2+|W_F(\omega_1)W_2(\omega_1)|^2}. \quad (37)$$

If

$$|W_S(\omega_1)W_1(\omega_1)| \gg |W_F(\omega_1)W_2(\omega_1)|, \quad (38)$$

Then $W(\omega_1)\approx|W_S(\omega_1)W_1(\omega_1)|=K$.

In this case, the disturbance suppression at this frequency $H(\omega_1)$ will be K times, and the remaining disturbance will be equal to $H(\omega_1)/K$. In this case, the result of calculating the control error will be equal to

$$\begin{aligned} E(\omega_1) &= \mathrm{V}(\omega_1) \\ &\quad - \frac{[W_S(\omega_1)W_1(\omega_1)+W_F(\omega_1)W_2(\omega_1)]H(\omega_1)}{K} \\ &\approx \mathrm{V}(\omega_1) - H(\omega_1) - \frac{W_F(\omega_1)W_2(\omega_1)H(\omega_1)}{K} \\ &\approx \mathrm{V}(\omega_1) - H(\omega_1). \end{aligned} \quad (39)$$

The neglect of the last term is carried out on the basis of relation ***(Equation 38)****.*

The interpretation of this mathematical relationship is that in the frequency range where the transfer function of the slow loop is significantly greater than that of the fast loop, the presence of the fast loop does not affect the magnitude of the control error, and therefore, the fast loop does not affect the overall performance of the loop. Similar statements can be used to demonstrate that, in the frequency range where the slow loop's transfer function is significantly greater than that of the slow loop, the slow loop does not affect the overall performance of the loop. In the frequency range

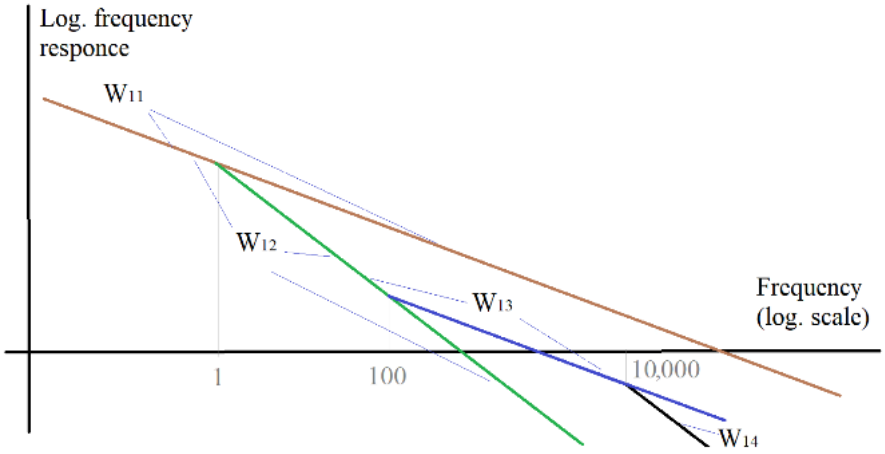

Figure B1. Graphs of transfer functions $W_{11}(\omega)$, $W_{12}(\omega)$, $W_{13}(\omega)$and$W_{14}(\omega)$.

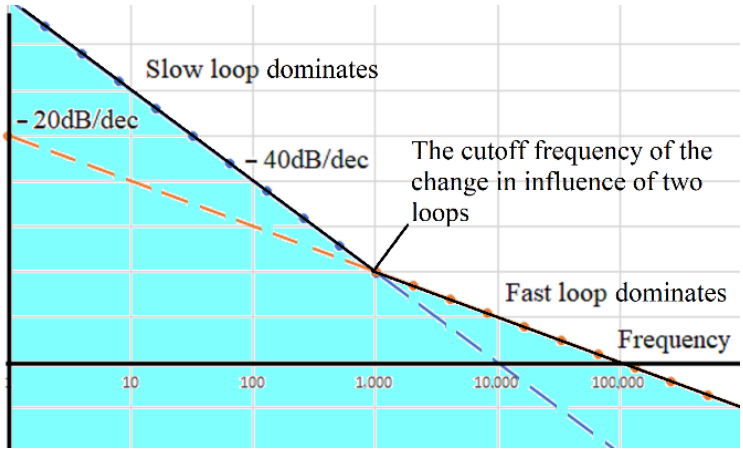

Figure B2. The equivalent transfer function of two parallel circuits is approximately equal to the envelope of these two functions, and at the intersection point of the graphs is 6 decibels higher.

where these transfer functions are comparable, both loops contribute comparably to disturbance suppression and target tracking. Since the logarithm of the sum of two values, one of which is much larger than the other, is approximately equal to the logarithm of the larger value, when the transfer functions of the two loops are arranged as shown in ***Figure 4****, the equivalent overall transfer function is the upper envelope of the two graphs, as shown below in* ***Figure B2****. At the point where these functions intersect, the equivalent overall transfer function is 6 dB higher, since the logarithm of the sum of two equal quantities is equal to the logarithm of twice one of the quantities, so it is equal to the logarithm of that quantity plus the logarithm of two* ***Figure B2****.*

$$\lg(A+A) = \lg(2A) = lg2 + lgA \approx 0,3010 + lgA.$$

$$20\lg(A+A) \approx 20 \times 0,3010 + 20lgA \approx \approx 20lgA + 6dB \quad .$$

The effectiveness of the loop can be assessed by the shape of the positive portion of the logarithmic amplitude–frequency characteristic. The value of this characteristic at any frequency describes the disturbance suppression coefficient at that frequency, and the reciprocal characterizes the residual relative error in transmitting the reference from the system input to the output. For example, where the value of this transfer function is 1,000, the disturbance is suppressed by a factor of 1,000, and the reference is transmitted with an error of 0.001. Using two circuits allows, for a given system bandwidth limit, which is determined by the intersection of the total logarithmic amplitude–frequency characteristic with the abscissa, to ensure a sharper rise in this characteristic in the low-frequency range. In other words, the higher the characteristic shown in ***Figure 6*** *is above the abscissa, the better the system. But there is an upper frequency at which the delay of the object becomes critically large, $|\varphi| > \pi$ rad. For this frequency, the transfer function of the object must have a coefficient less than $|W(\varphi)| < -12$ dB, and the intersection of this graph with the abscissa axis must occur at an angle -20 dB/dec, there are known cases with ensuring a non-multiple of twenty intersection angle of the order of -30 dB/dec, which is called non-integer integration or one and a half integration, but in this case the system's stability margin is sharply reduced.*

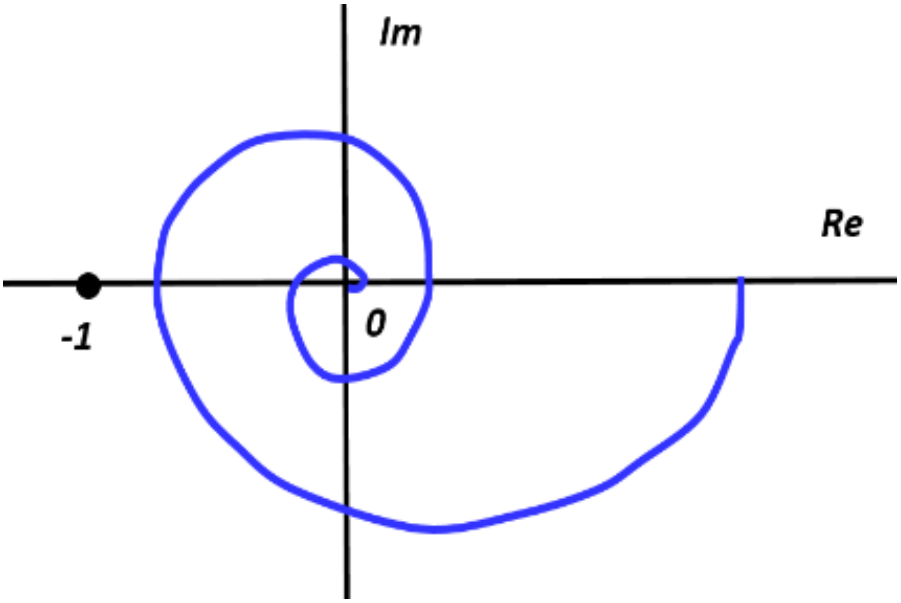

Figure C1. Hodograph of a stable system that does not cover the point {−1; j 0}.

Appendix C

The Nyquist stability criterion, as well as its logarithmic interpretation, is widely used to analyze the stability of closed-loop systems. The plot of the frequency response of a circuit in its conditionally open form on the complex plane, called the hodograph, should not cover the point {−1; j0}. If it does not cover this point, the system is stable ***(Figure C1)****, if it covers this point* ***(Figure C2)****, then the system is unstable.*[1,2] *If the system has an integrator, the hodograph begins on the imaginary axis at minus infinity* ***(Figure C3)****. According to* ***Figure C4****, the system is also stable. Even though such a system seems to cover the critical point, it still does not. If we lay a rope along the hodograph line and put a finger at the critical point {−1; j0}, and then pull the ends of the rope, then it will not "catch" the finger. Only in the example according to* ***Figure C2*** *the loop "catches" the finger; only the system with the hodograph according to* ***Figure C2*** *of all four examples is unstable, and the systems according to* ***Figures C1****, C3, and C4 are stable.*

In our paper, we use logarithmic amplitude–frequency characteristics for our reasoning.

In the representation of separate amplitude and frequency responses on a logarithmic scale, the length of the vector drawn from the origin to each point on the hodograph is shown on the same axes as the phase, which determines the angle of rotation of such a vector. A circle with a radius of unit length on a logarithmic scale is in this case transformed into the abscissa axis, the angle −180° is transformed into a corresponding line on the phase trajectory graph, parallel to the abscissa axis, the hodograph does not cover the point {−1; j0} if the amplitude response lies above the abscissa axis only in the region where the phase response has not yet fallen below the value −180° (−π radians). But a widely known theory reasonably asserts that if, in the region where the amplitude characteristic lies above the abscissa axis, the phase characteristic still falls below the level of −180° (−π radians), but then returns back to the region above this level and remains there until the amplitude characteristic falls below the abscissa axis, then the system will still be stable.

A typical pair of amplitude–frequency and phase–frequency response graphs along the same axes is shown in ***Figure C5****. Specifically, this characteristic is recommended for the stabilization circuit of a focus tracking system in an optical disk drive (a standard requirement), which levitates a magnetically suspended lens to stabilize the focal length with an error of no more than 1 μm when the x-axis intersection frequency (the unity gain frequency of the circuit) is 12 kHz. The desirability of this characteristic is justified in standards written before 1985. We have manufactured similar systems with such parameters for many optical systems requiring focus tracking. Experience has repeatedly confirmed the feasibility of this type of transfer function. The theory also states that the pure lag element affects only the phase response, adding a phase shift equal to the product of the frequency and the time constant of this element, as shown in* ***Figure C6****. Thus, at low frequencies, the lag element has no effect or only a minor one, but at high frequencies, it has a very significant, fatal effect. The influence of this element begins where the product of this element's time constant and the frequency contributes to the phase delay by more than 1%; that is, this product exceeds 0.015 radians. And the fatal effect occurs when the phase shift due to the lag element leads to an uncompensable lag, even by a differentiating element; this lag exceeds π/4 radians. The theory also states that in the region where the delay is absent or insignificant, the phase shift is uniquely determined by the slope of the logarithmic amplitude–frequency characteristic. A slope of −20 dB/dec corresponds to a phase shift of 0.5π radians. Therefore, providing a section with a slope of −180°*

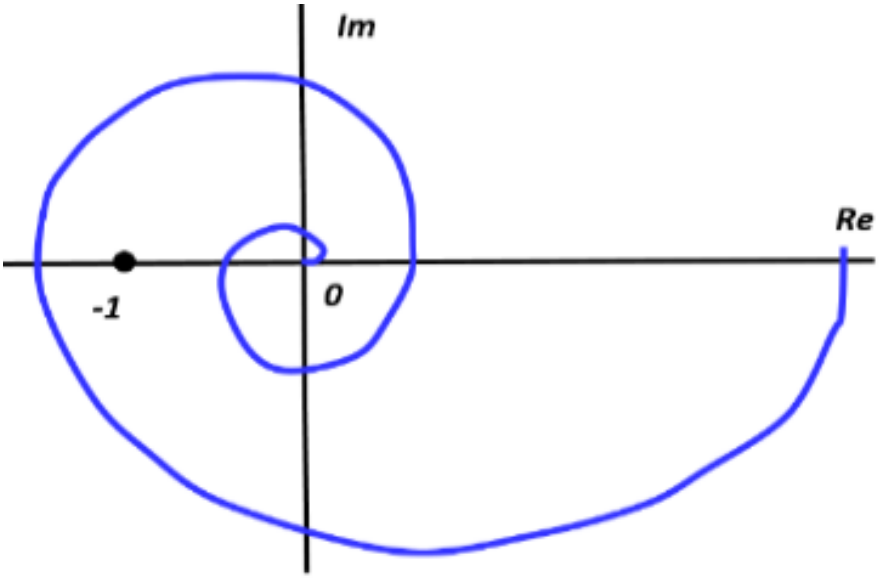

Figure C2. Hodograph of an unstable system that covers the point {−1; j 0}.

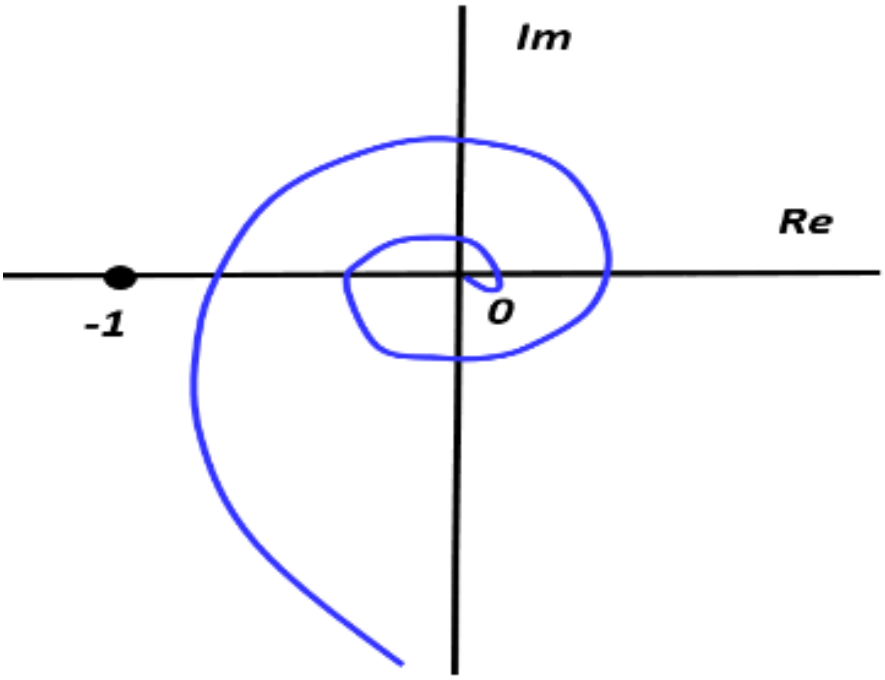

Figure C3. Hodograph of a stable system with an integrator that does not cover the point {−1; j 0}.

(i.e., π radians) intersecting the x-axis, provided the influence of the delay is small in this frequency range, ensures system stability. Thus, the recommended form of this characteristic, shown in ***Figure C1*** *in the article, is an indicator of system stability under the condition of a small influence of the delay. The stability margin when using this method is determined by the length of this section; it is usually required that its length in both directions be at least 12 dB. This also requires constructing an accurate phase-frequency characteristic due to the presence of a delay element. However, this method is numerical and relies on approximate engineering calculations and graphs, although it has proven itself remarkably successful. Over the past 30 years, this method has been used less frequently because stability and safety margins can be more easily verified using numerical simulation. However, this method is quite useful for substantiating the theory of controller structural synthesis, that is, the theory of structure selection. It is on this theoretical foundation that a structure with a steeper slope in the low-frequency part of the frequency response was proposed, since, according to the theory, this does not compromise stability.*

Therefore, the discussion of designing higher-order slow loops is not intuitive; it is formally established.

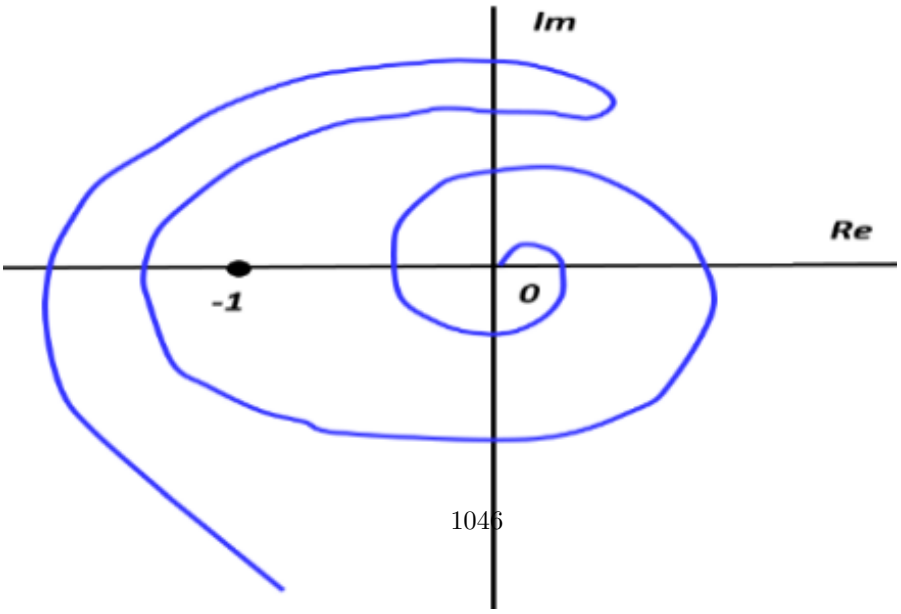

Figure C4. Hodograph of a stable system with an integrator, which, however, does not cover the point $\{-1; j\ 0\}$, such a system is also stable, which is a well-known theoretical fact.

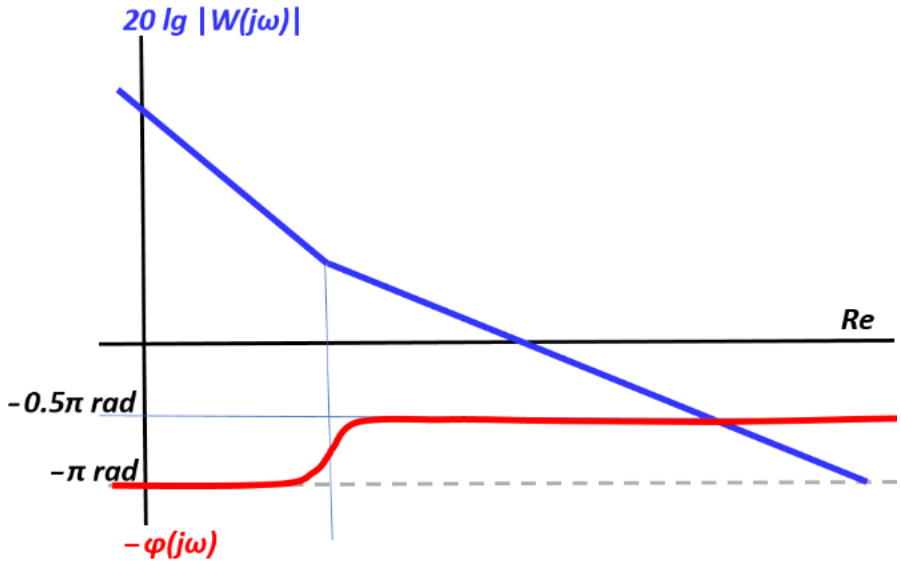

Figure C5. Characteristic amplitude-frequency (blue line) and phase-frequency (red line) characteristics of the open loop of a stable system.

References

31. *Kodkin V, Anikin A, Kuznetsova E. Efficiency of Applying the Nyquist and VM Popov Criteria for Stability Analysis of Linearized Automatic Control Systems in Electromechanics and Power Engineering. Energies. 2023;16(2):872. https://www.doi.org/10.3390/en16020872.*

32. *Tsirlin AM, Balunov AI. Optimal Control of Technological Processes. Processes. 2023;11(6): 1835. https://www.doi.org/10.3390/pr11061835.*

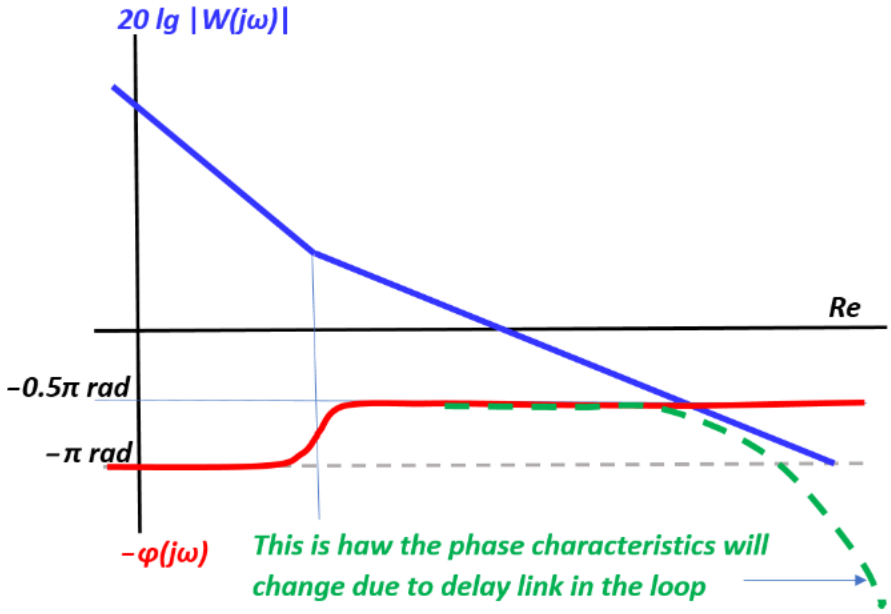

Figure C6. The same as **Figure C5**, but the green line shows the characteristic change in the phase–frequency characteristic due to the presence of a delay link in the object model.

An International Journal of Optimization and Control: Theories & Applications (https://accscience.com/journal/ijocta)